

FORMATION MOTION PLANNING FOR PAYLOAD TRANSPORT BY MODULAR WHEELED MOBILE MANIPULATORS

by

Rajankumar M Bhatt

A thesis submitted to the
Faculty of the Graduate School of
State University of New York at Buffalo in partial
fulfillment of the requirements for the degree of

Master of Science

Date

December 12, 2003

To my family
Pappa, Mom,
Bhai, Bhabhi
and *Vrusti*

Acknowledgements

I would like to express my sincerest gratitude to my advisor, Dr. Venkat Krovi, for giving me an opportunity to work under him. He was not only my mentor but also a friend and on occasions, a guardian guiding me through whenever I needed the most. His excellence in the field and enthusiasm to work extended hours has always been a source of inspiration.

Special thanks to the committee members, Dr. John Crassidis and Dr. Kemper Lewis for reading through my thesis and making a number of helpful suggestions.

I am obliged to Chin Pei Tang for all the discussions and for his painstaking effort of going through the text of this thesis. Pravin Nair was the best companion inside and outside the lab. Seung-Kook Jun was always available for any kind of help and inspiration I ever needed. Narayana Sundaram, I miss your joyful company from the day you left ARMLab. I would also like to thank Leng-Feng, Glenn, Ajay, Dan, Harpreet, Talib and all other present and past ARMLab members for making it such a nice place to work in.

I would like to thank Chetan for his appetizing food. Special thanks to Ravishankar who spent nights understanding my work and giving me suggestions on my presentation. I would also like to thank my past housemates: Amit, Mitul, Urmil, Samir, Burzin, and Hardik.

Amid stressful hours of writing thesis, entertaining jokes during Starbucks visits with Ashwin and Chin-Pei Tang were best entertainment that I can hope for. I would also like to thank Mrs. Dr. Krovi, Dr. Chii-Chuan, Deepak, Aniruddha, Tsui-Ling, Annapurna,

Yugendra, Eric and all friends and fellow Buffaloites, there are way too many to list here, for those happy memories which I shall carry along with me wherever I go.

Finally, I want to thank my family, *Pappa, Mom, Bhai, Bhabhi* and *Vrusti* for each and every thing that they have done for me. Their perpetual encouragement, support and faith in me even during my absence were vital aspects that led towards the completion of this thesis. I dedicate this work to them.

Table of Contents

| | |
|---|-------------|
| Acknowledgements | iii |
| Table of Contents..... | v |
| Abstract..... | viii |
| List of Figures | x |
| Chapter 1..... | 1 |
| Introduction..... | 1 |
| Scenario | 3 |
| Modularity..... | 4 |
| Issues..... | 6 |
| State-of-the-Art | 7 |
| Contributions | 8 |
| Thesis Organization | 10 |
| Chapter 2..... | 11 |
| Mathematical Background..... | 11 |
| Homogeneous Transforms | 11 |
| Two-link Manipulator Kinematics | 16 |
| Jacobian Based Performance Measures | 19 |
| Riemannian Metrics Based Performance Measures | 22 |
| Curve Representation and Geometric Invariants..... | 24 |

| | |
|---|-----------|
| Chapter 3..... | 31 |
| Mobile Manipulators..... | 31 |
| Wheeled Mobile Robot..... | 31 |
| Mobile Manipulator | 35 |
| Formations..... | 41 |
| Motion Parameterization | 45 |
| Chapter 4..... | 47 |
| Motion Planning | 47 |
| Serret-Frenet Frame | 48 |
| Curvature Of A Curve | 48 |
| Rigid (and Non-rigid) Virtual Structure | 50 |
| Geometric Motion Planning Strategy..... | 51 |
| Chapter 5..... | 55 |
| Formation Motion Planning | 55 |
| Problem Formulation..... | 55 |
| Screw Motion..... | 58 |
| Non-Screw (Sinusoidal) Motion..... | 63 |
| Chapter 6..... | 67 |
| Formation Payload Transport | 67 |
| Type III: R Mobile Manipulator Module..... | 67 |
| Type II: RR Mobile Manipulator Module | 69 |

| | |
|--|-----------|
| Type I: RRR Mobile Manipulator Module | 70 |
| Equivalence of Parameterizations | 72 |
| Chapter 7 | 75 |
| Conclusions and Future Work..... | 75 |
| Summary and Conclusion..... | 75 |
| Future Work..... | 76 |
| Bibliography | 78 |

Abstract

The goal of this thesis is to develop team-optimal kinematic motion plans for all members of a team of Wheeled Mobile Robots (WMRs) moving in formation. The structure provided by the formation paradigm reduces the problem of simultaneous motion planning for the entire team into a staged motion planning problem. Motion plans are created first for a single WMR from which all other team members subsequently derive their individual motion plans. There is still considerable freedom, however, in terms of selection of relative positions within the formation which affects the performance of the team as a whole. The principal contributions of this thesis are in: modeling such formations of WMRs forming the team; determining the “best formation” to trace desired planar paths; and concurrently projecting the team-optimal motion plans into individual motion plans for all members of the team.

Specifically, this is achieved by coupling kinematic motion planning methods developed for individual WMRs with creation/evaluation of performance measures developed for the overall formation. The preferred kinematic motion planning method used in this thesis is the Geometric Motion Planning Strategy (GMPS) wherein each WMR is aligned with an induced vector field. This strategy is extended to the formation by considering a preferred “team-fixed frame” and aligning all WMRs within the team with the corresponding induced helicoidal velocity vector-field. Different relative position of each mobile robot within the formation induces different motion plans for individual WMRs. Special emphasis is placed on developing quantitative measures of formation quality, from appropriate metrics on $SE(2)$, that permits subsequent optimization of the relative positions of mobile robots within the formation for given tasks. Case studies for three nonholonomic

WMRs maneuvering along certain desired paths are presented. For the cases when analytical expressions are possible, the expressions for the optimal configuration of the formation are derived analytically for comparison with the numerical results.

Further, the formation-based motion planning scheme developed for an unconstrained team of WMRs is then extended to also treat a team of physically constrained WMRs. In particular, we show the equivalence between the two cases, one when the module is moving in formation without stringent physical constraints that arises due to the payload, and other when the module within the formation is cooperating physically to transport a payload from a home location to destination location.

List of Figures

| | |
|--|-----------|
| FIGURE 1-1 CLEANING BY COOPERATION (ROUGEAUX AND ZELINSKY) | 1 |
| FIGURE 1-2 UNCONSTRAINED AND PHYSICALLY CONSTRAINED TEAM OF MOBILE ROBOTS | 2 |
| FIGURE 1-3 TYPICAL DOLLY USED BY FURNITURE MOVERS..... | 4 |
| FIGURE 2-1: HOMOGENEOUS TRANSFORMS BETWEEN FIXED FRAME {F} AND MOVING FRAME {M} | 11 |
| FIGURE 2-2: TWO LINK MANIPULATOR | 16 |
| FIGURE 2-3: MANIPULABILITY ELLIPSOID FOR A TWO LINK PLANAR MANIPULATOR..... | 20 |
| FIGURE 2-4: ARC-LENGTH AS A FUNCTION OF NUMBER OF SEGMENTS..... | 28 |
| FIGURE 3-1: A WHEELED MOBILE ROBOT..... | 31 |
| FIGURE 3-2: A MOBILE MANIPULATOR | 36 |
| FIGURE 3-3: A FORMATION OF WHEELED MOBILE ROBOTS | 42 |
| FIGURE 3-4: A FORMATION OF MOBILE ROBOTS..... | 44 |
| FIGURE 4-1: SERRET-FRENET FRAME AND CURVATURE | 47 |
| FIGURE 4-2: VISUALIZATION OF INSTANTANEOUS CENTER OF ROTATION CONSTRAINT..... | 52 |
| FIGURE 5-1: UNCONSTRAINED FORMATION OF WHEELED MOBILE ROBOTS..... | 56 |
| FIGURE 5-2: CREATION OF SECTORS FOR FEASIBLE LOCATIONS OF INDIVIDUAL ROBOTS | 57 |
| FIGURE 5-3: ANALYTICAL SOLUTION FOR OPTIMAL CONFIGURATION..... | 60 |
| FIGURE 5-4: ANALYTICAL RESULTS FOR SCREW MOTION | 62 |
| FIGURE 5-5: OPTIMAL CONFIGURATION FOR FOLLOWING A SCREW MOTION (OBTAINED NUMERICALLY) | 63 |

| | |
|---|-----------|
| FIGURE 5-6: ANALYTICAL RESULTS FOR NON-SCREW (SINUSOIDAL) MOTION..... | 65 |
| FIGURE 5-7: COMPARISON BETWEEN NUMERICAL AND ANALYTICAL VALUES OF κ | 66 |
| FIGURE 6-1: FORMATION OF TYPE III MODULES WITH A PAYLOAD..... | 68 |
| FIGURE 6-2: FORMATION OF TYPE II MODULES WITH A PAYLOAD | 69 |
| FIGURE 6-3: FORMATION OF TYPE I MODULES WITH A PAYLOAD (PARAMETERIZATION LOCAL TO EACH MOBILE MANIPULATOR)..... | 70 |
| FIGURE 6-4: AN ALTERNATE PARAMETERIZATION OF FORMATION OF TYPE I MODULES (TASK FRAME BASED PARAMETERIZATION) | 72 |

Chapter 1

Introduction

Over the past two decades, the incorporation of cooperation among multiple mobile agents has received considerable research attention for many reasons. Cooperation has been a key factor to the success of most human endeavor and similar incorporation of cooperation in robotic systems is critical for the next generation of robotic applications. Interest in cooperating systems arises when the tasks to be accomplished may be too large and complex for one single system to accomplish or building smaller systems instead of one single larger system may be easier, cheaper, more flexible, and more reliable.

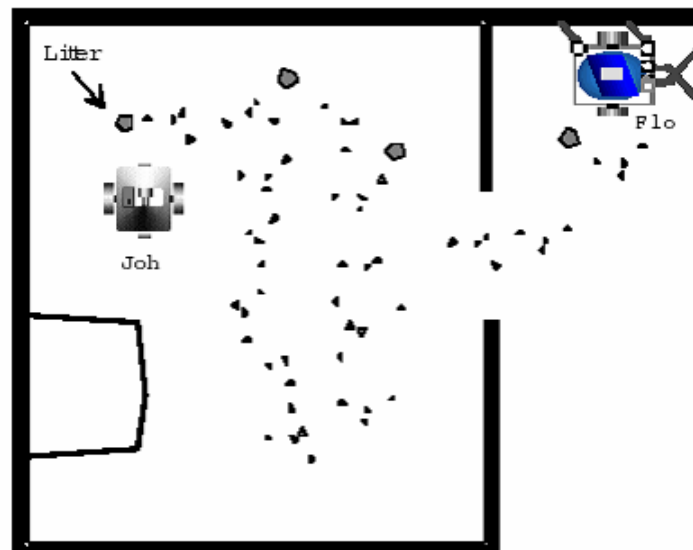


FIGURE 1-1 CLEANING BY COOPERATION (ROUGEAUX AND ZELINSKY)

While such cooperating systems can potentially have many advantages, the implementation of such cooperation creates many challenges. Principal among these is the requirement for coordination between the multiplicities of agents and in achieving this in a decentralized scalable manner. In recent years, there has been considerable interest in creating such cooperation between decentralized and distributed mobile robotic systems. A bulk of these efforts has focused on information-level cooperation in applications such as foraging, reconnaissance and map-building. This is illustrated in the example as shown in Figure 1-1.

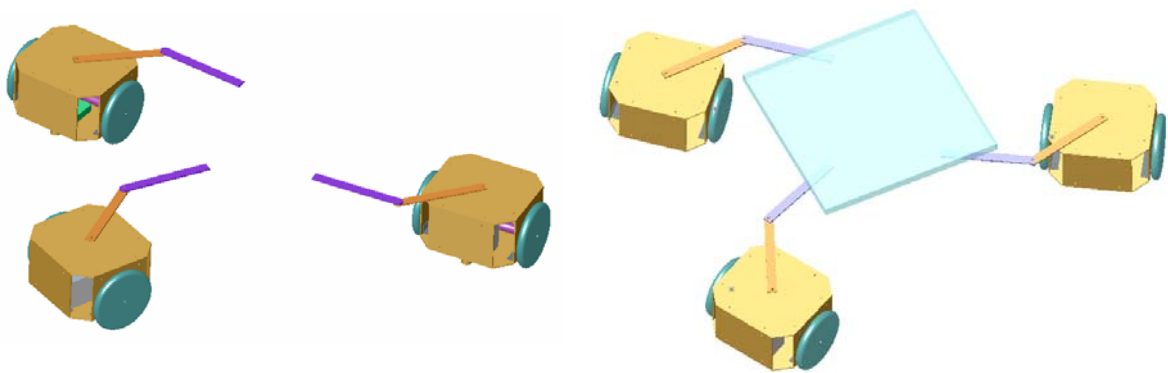


FIGURE 1-2 UNCONSTRAINED AND PHYSICALLY CONSTRAINED TEAM OF MOBILE ROBOTS

The multiple distributed and decentralized agents can search for a desired target simultaneously mapping their immediate surroundings and exchanging collected information in order to complete the task in a much shorter time span than may be possible with a single agent. Our focus is on the part that comes after such a target may have been located. We envisage a situation where these agents can now attempt to lift this target component onto their end-effector and combinedly relocate it to its final

destination. Thus, our focus is on the physical cooperation that becomes necessary to achieve these objectives.

Despite advances in state-of-the-art and considerable efforts over past few decades, the incorporation of physical cooperation into distributed and decentralized robotic systems still remains a challenge. We note that such physical cooperation places far more stringent constraints on all aspects of design, analysis and control of such systems. The following scenario illustrates many of these challenges and help further enhance the understanding of the nature of the desired physical cooperation.

Scenario

Consider the illustrative scenario of household furniture movers required to move a large piece of furniture. Traditionally, such movers employ variable numbers of modular wheeled dollies as shown in Figure 1-3, as determined by the payload. These are positioned at suitable locations, to ensure mobility, stability and load-distribution within the aggregation, which is then steered away as a single composite system. Occasionally, additional dollies may be added or the relative locations of existing dollies may be readjusted to avoid obstacles or to enhance overall performance. A significant enhancement would be obtained if these wheeled dollies, with added intelligence and autonomy, could cooperate to either assist the human operator or autonomously perform this overall payload transport process.

Thus, our guiding vision is to create an overall framework for payload manipulation – with a “fleet of individual semi-autonomous wheeled mobile modules”, combined together flexibly to create a composite system that possesses the ability to

“reconfigure to enhance performance”. The increased flexibility and robustness, derived from replacing a single large material handling device by a fleet of smaller, less-capable but inexpensive modular systems achieving equal or better overall performance, make such composite systems very attractive.



FIGURE 1-3 TYPICAL DOLLY USED BY FURNITURE MOVERS

Our emphasis is on physical collaboration in such decentralized but physically-coupled collectives which impose more stringent constraints than encountered in many of the concurrent collective robotics efforts that focus on information collaboration for reconnaissance, map building etc. Our proposed application arenas would range from industrial applications in which suitable numbers of such modules can be tasked to manipulate variable-sized payloads in the absence of gantry systems to extra-terrestrial applications in which individual “rover” modules sent on separate missions can cooperate to support planetary colonization efforts. In particular, our focus is on creating and retaining modularity within an overall system that is capable of reconfiguration for the reasons to be discussed below.

Modularity

The concept of modularity, as applied in modern systems, is based on the hypothesis that a collective system formed by number of smaller modules performs “better” than one large system. Each module, thus formed, would be simpler than a large

complex system and thus, easier to “design” and “control”. An important consequence of the adoption of such a modular approach is the creation of redundancy.

Redundancy, defined as the ability of the system to overcome lost capabilities with available resources, can also be easily incorporated in a modular system to enhance the load distribution and robustness, thus improving the overall reliability of the system. If one of the modules fails, such module can be replaced by another module. Modular introduction of redundancy in a system by keeping inventories of the smaller, less expensive modules is also less costly compared to the large complex system. Decentralization of the control of the system may also be possible, which has the benefit of simplifying the control algorithm.

With a modular system, it is possible to readjust and reconfigure the system to redistribute some performance measure like load, stability, manipulability or energy. The ability of the system to dynamically reconfigure itself can also be used to avoid obstacles and to accommodate for external disturbances. By attaching a payload to individual modules endows the system with redundant sensing and redundant actuation. Redundancy introduced in terms of redundant sensing can be used to detect such external disturbances whereas the redundancy introduced in terms of redundant actuation can be used to avoid singular configurations. Since modularity introduces “more choices”, there are many possible ways in which a given task can be accomplished. Hence, it is necessary to resolve these choices and determine the “best way” to accomplish a given task.

Issues

As seen above, modularity gives many advantages but also brings in issues which need to be handled. While a broad classification into *design related issues* (which need to be resolved prior to manufacture) and *control related issues* (which can be resolved after the system has been constructed) is useful, we note that these are highly coupled issues. Thus, while we focus principally on design related issues, the control aspects nevertheless greatly affect and influence our design choices.

We view design as the process of systematically creating choices, evaluating these choices and then systematically eliminating poor choices to obtain the best design. In this light, we note that the incorporation of modularity now expands the initial availability of choices significantly. In particular, we focus on parametric generation of such choices. The problem includes both, discrete choices like number and type of joints, number and type of wheels, type of motors etc as well as continuous parametric choices like length of links, radius of wheels, distance between wheels, etc. Other choices are created by the nature of addition of modules into a system. Many feasible configurations are possible in order to accomplish a given task of moving in formation from one location to another location. Hence, it is necessary to resolve this redundancy and find the “best” feasible solution.

Thus, in order to evaluate these choices, some performance criterion, either local or global, needs to be created to facilitate determination of the best choice. The selection of many of these parameters can significantly influence the system performance. For example, closed chains introduce constraints and redundancy. A variety of redundancy resolution schemes have been proposed in the literature based on Jacobian analysis. The

configuration of a mechanism at any instant depends on its previous configurations. The redundancy thus arising due to configuration is called kinematic redundancy. Other examples of such criteria could include load distribution, stability, manipulability, energy, controllability etc. Local criterion may conflict with global and vice versa. While a local determination of a best configuration for an individual module is possible, it may not be the best configuration for the system as a whole (even using the same criterion). But, while there are potentials of conflict between multiple criteria, we know that the available design space is considerable.

State-of-the-Art

Several approaches to coordination of fleets, schools and teams of robotic-agents are reported in the literature – see (Arkin and Bekey, 1997; Cao, Fukunaga and Kahng, 1997; Parker, 2000) for surveys. “Behavior”-based control adherents address the complexity of multi-agent coordination by decomposing the high-level goals into primitive tasks and implementing simple controllers for them, with the notion of an emergent intelligence as the sets of interacting behaviors grow. The benefits of such behavior based control include ease of decentralization, limited communication needs and surprisingly good performance using relatively simple behaviors (Balch and Arkin, 1998; Parker, 1998). However, a systematic method for synthesizing desired emergent behavior and analyzing its performance/robustness has proven difficult.

In parallel, the “formation” paradigm has also emerged as a convenient mechanism for abstraction and coordination with approaches ranging from leader-following (Desai, Ostrowski and Kumar, 2001; Wang, 1991), virtual structures (Beard, Lawton and Hadaegh, 2001; Lewis and Tan, 1997) and virtual leaders (Leonard and

Fiorelli, 2001; Ogren, Fiorelli and Leonard, 2002). The group control problem now reduces to a well-known single-agent control problem from which the other agents derive their control laws but requires communication of some coordination information. The formation paradigm has evolved to allow prescription of parameterized formation maneuvers (Fiorelli and Leonard, 2002; Young, Beard and Kelsey, 2001) and group feedback (Egerstedt and Hu, 2001; Ogren, Egerstedt and Hu, 2002). From these seemingly disparate approaches, a dynamic system-theoretic perspective has emerged for examining the decentralized multi-agent “behavioral control” of “formations” (Egerstedt and Hu, 2001; Ogren, Egerstedt and Hu, 2002; Lawton, Young and Beard, 2000; Olfati-Saber and Murray, 2003) and our work is set in this context.

Contributions

Inclusion of Nonholonomic Constraints in Planning Phase

Many formation planning approaches treat the mobile agents simply as point objects with unconstrained motions in \mathbb{R}^2 . Nonholonomic constraints, if considered, are tackled by defining a suitable end-effector point for the wheeled base and applying nonlinear input-output feedback linearization techniques. The planning problem is converted back into one of planning the unconstrained Cartesian motions of this end-effector point in \mathbb{R}^2 (with guaranteed-stable zero dynamics) (Young, Beard and Kelsey, 2001). Motion plans are first created for the end effector positions of the multiple robots within the formation and in a second stage translated into motion plans for each individual robot with respect to its end effector.

In contrast, we develop kinematic motion plans for formations of differentially driven mobile robots, while retaining their full nonholonomic form. In particular, we

consider these differentially driven mobile robots to be attached to the virtual structure at their center of axle (a point that traditionally has been avoided because of the singularity induced in the input-output feedback linearization). For any given (planar) path, we first determine the instantaneous motion of the Serret-Frenet frame and the corresponding pole of the motion. Aligning a “team-fixed frame” with this Serret-Frenet frame now induces a helicoidal velocity vector field for the vertices of the virtual structure. Our planning algorithm for the individual mobile robots then aligns the forward direction of travel with this helicoidal velocity vector field.

Determination of Optimal Configuration of the Overall Formation

The relative position of each mobile robot within the virtual structure induces different motion plans for the individual mobile robots. By using a suitable metric, defined on the motions of each mobile robot, we evaluate the performance of such induced motion plans. These performance metrics in cumulative form or individual form are used to optimize the overall formation (i.e. their relative positions) for performing a given task. This optimization can be carried out for a given instant of time or for the entire motion. While a global formation optimization can be carried out for an entire prescribed path, we also discuss the creation of local optimization (at a given instant of time) that is well suited for online implementation.

Application to the Payload Transport Case

When the MMs are carrying a payload, the payload on top of the MMs forms a parallel structure. This introduces additional redundancy and more stringent constraints in the system. We show two different ways to parameterize system with a payload: centralized task frame based parameterization which is useful for centralized

implementation and individual MM module based parameterization which is useful for a decentralized implementation of planning algorithm.

Thesis Organization

The organization of this thesis is as follows: In Chapter 2, we briefly discuss the mathematical tools used in this thesis. We first discuss the homogeneous transforms and their underlying group-theoretic background followed by a brief discussion on manipulator modeling and various Jacobian based and group-based performance measures and finally curves modeling.

In Chapter 3, we develop the terminology and notation to model the individual Wheeled Mobile Robot (WMR), the MM and the virtual structure. We also develop the Jacobian matrices for WMR and MMs using the traditional approach and twist based approach. Finally, we present a brief summary on Motion Parameterization.

In Chapter 4, we develop the GMPS that considers the nonholonomic constraints of the MMs. In Chapter 5, a case study of 3 mobile robots, moving in formation, is considered and we present the results of the application of GMPS as developed in Chapter 4.

In Chapter 6, we discuss the implementation of the GMPS to transport a payload using the Manipulator Modules described in Chapter 3 and equivalence of two different types of configuration parameterizations. In Chapter 7, we conclude the thesis and give directions for future work.

Chapter 2

Mathematical Background

A brief discussion of the mathematical tools used in this thesis is presented in this chapter. This includes a brief summary of homogenous transforms, their underlying group-theoretic background, manipulator modeling, Jacobian based performance measures, group-based performance measures and curve modeling. The reader is encouraged to the cited references for a more detailed treatment of these topics.

Homogeneous Transforms

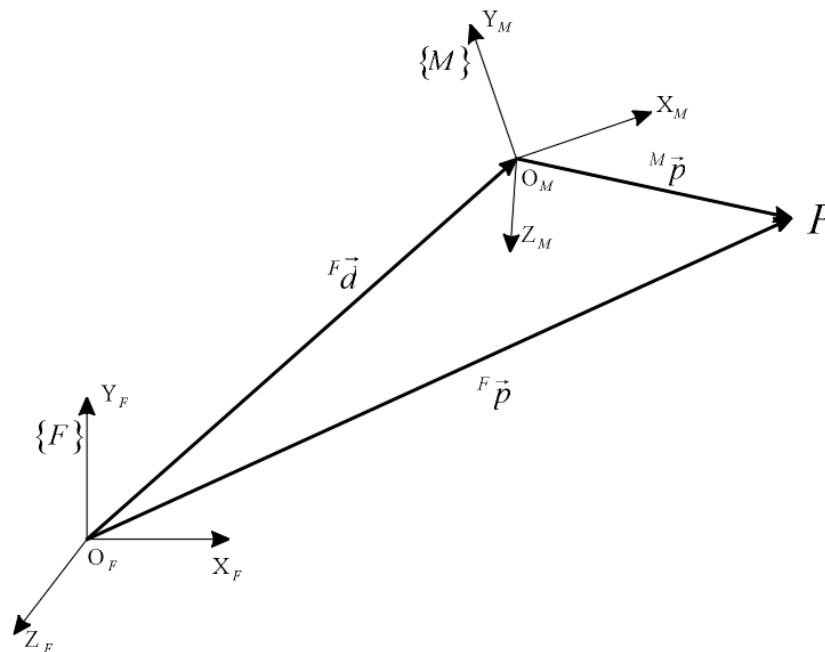


FIGURE 2-1: HOMOGENEOUS TRANSFORMS BETWEEN FIXED FRAME {F} AND MOVING FRAME {M}

Consider the set of frames as shown in Figure 2-1. The fixed base frame with origin, O_F , and the three orthonormal axes, X_F , Y_F and Z_F , is denoted by $\{F\}$ while a moving frame, with its origin at O_M and the three axes X_M , Y_M and Z_M is denoted by $\{M\}$. The position vector of O_M relative to O_F , expressed in $\{F\}$ is denoted by ${}^F\vec{d}$. The unit vectors in direction of X_M , Y_M and Z_M , expressed in $\{F\}$, are ${}^F\hat{x}_M$, ${}^F\hat{y}_M$ and ${}^F\hat{z}_M$ respectively. The matrix ${}^F\mathbf{R}_M$ captures the relative orientational displacement of frame $\{M\}$ with respect to frame $\{F\}$ and can be expressed as:

$${}^F\mathbf{R}_M = \begin{bmatrix} {}^F\hat{x}_M & {}^F\hat{y}_M & {}^F\hat{z}_M \end{bmatrix} \quad 2.1$$

The set of all such orientational displacements in three dimensions forms a group, denoted as $SO(3)$ and defined as:

$$SO(3) = \{\mathbf{R} \mid \mathbf{R} \in \mathbb{R}^{3 \times 3}, \mathbf{R}^T \mathbf{R} = \mathbf{R} \mathbf{R}^T = \mathbf{I}, \det(\mathbf{R}) = +1\} \quad 2.2$$

${}^M\vec{p}$ is the position vector of point P expressed in the coordinate system of $\{M\}$. The corresponding coordinates of P expressed in the base frame $\{F\}$, ${}^F\vec{p}$, can be written as:

$${}^F\vec{p} = {}^F\mathbf{R}_M {}^M\vec{p} + {}^F\vec{d} \quad 2.3$$

Equation 2.3 may be expressed in homogeneous form as

$$\begin{bmatrix} {}^F\vec{p} \\ 1 \end{bmatrix} = \begin{bmatrix} {}^F\mathbf{R}_M & {}^F\vec{d} \\ 000 & 1 \end{bmatrix} \begin{bmatrix} {}^M\vec{p} \\ 1 \end{bmatrix} = {}^F\mathbf{A}_M \begin{bmatrix} {}^M\vec{p} \\ 1 \end{bmatrix} \quad 2.4$$

where the 4×4 matrix ${}^F A_M$ is called the homogeneous transform matrix. Equation 2.4 has an alternate interpretation as the equation of a general rigid body spatial displacement that displaces a rigid body from an initial configuration coincident with $\{F\}$ to its current configuration $\{M\}$. The set of all such general rigid body spatial displacements forms a group called $SE(3)$, the special Euclidean group of three-dimensional rigid body displacements and is denoted as:

$$SE(3) = \left\{ {}^F A_M \mid {}^F A_M = \begin{bmatrix} {}^F R_M & {}^F \vec{p} \\ 000 & 1 \end{bmatrix}, {}^F R_M \in SO(3), {}^F \vec{p} \in \mathbb{R}^3 \right\} \quad 2.5$$

Elements of $SE(3)$ satisfy both the requisite axioms of an algebraic group and the continuity requirements in terms of being locally diffeomorphic to Riemannian manifold and thus $SE(3)$ has the structure of a matrix Lie group. The set of rigid body displacements in a plane form a proper subgroup of $SE(3)$ and is denoted as ${}^F A_M \in SE(2)$ and expressed as:

$$SE(2) = \left\{ {}^F A_M \mid {}^F A_M = \begin{bmatrix} {}^F R_M & {}^F \vec{p} \\ 00 & 1 \end{bmatrix}, {}^F R_M \in SO(2), {}^F \vec{p} \in \mathbb{R}^2 \right\} \quad 2.6$$

In this thesis, we focus our attention principally on such planar rigid-body displacements.

Twist Matrix and Twist Vector

On a Lie group, the tangent space at the group identity has the structure of Lie algebra. The Lie algebra of $SE(2)$ is denoted by $se(2)$ and is given by:

$$se(2) = \left\{ \begin{bmatrix} \hat{\omega} & \bar{v} \\ 0 & 0 \end{bmatrix}, \hat{\omega} \in \mathbb{R}^{2 \times 2}, \bar{v} \in \mathbb{R}^2, \hat{\omega} = -\hat{\omega}^T \right\} \quad 2.7$$

Each 2×2 skew-symmetric matrix $\hat{\omega}$ can be uniquely identified with a vector $\bar{\omega} \in \mathbb{R}^1$. $\bar{\omega}$ and \bar{v} can together be expressed in vector form as an equivalent twist vector.

$$\bar{t} = \begin{bmatrix} \bar{\omega}^T & \bar{v}^T \end{bmatrix}^T \quad 2.8$$

Spatial and Body Fixed Twist Representations

Let ${}^F \dot{A}_M$ be the tangent vector in the tangent space of ${}^F A_M \in SE(2)$ which can be identified with an element of the Lie Algebra by either left translation or right translation. A body-fixed twist matrix ${}^M [{}^F T_M]$ can be obtained by left translation of such a tangent vector back to the identity element as:

$${}^M [{}^F T_M] = [{}^F A_M]^{-1} {}^F \dot{A}_M \quad 2.9$$

As noted earlier, a corresponding twist vector ${}^M \bar{t} = \begin{bmatrix} {}^M \bar{\omega}^T & {}^M \bar{v}^T \end{bmatrix}^T$ can be extracted from the twist matrix and physically interpreted as the linear and angular velocities of the origin of the moving frame $\{M\}$, expressed in the coordinates of the frame $\{M\}$. In such a case, the twist representation does not depend on the choice of inertial frame $\{B\}$ and hence is the preferred representation for locomotion systems.

A spatial-twist ${}^F [{}^F T_M]$ is obtained by right translation of the ${}^F \dot{A}_M$ back to the identity element and can be expressed as:

$${}^F \begin{bmatrix} {}^F T_M \end{bmatrix} = {}^F \dot{A}_M \begin{bmatrix} {}^F A_M \end{bmatrix}^{-1} \quad 2.10$$

The corresponding twist vector, ${}^F \vec{t} = \begin{bmatrix} {}^F \vec{\omega}^T & {}^F \vec{v}^T \end{bmatrix}^T$ may be similarly extracted from this twist matrix. Physically, ${}^F \vec{\omega}$ corresponds to the angular velocity of the body, while ${}^F \vec{v}$ corresponds to the velocity of a point on the moving body, which is instantaneously coincident with the origin of frame $\{F\}$, both expressed in frame $\{F\}$.

Similarity Transformation

Points and vectors can be transformed from one frame of reference to another using direct matrix multiplication by homogeneous transforms. However, two-tensors such as the inertia matrix, homogeneous transformation matrices or twist matrices can be transformed by means of similarity transformation from one frame to another frame.

Thus, the twist matrix T developed in frame $\{F\}$ can then be expressed in any arbitrary frame $\{N\}$ by a similarity transformation:

$${}^N \begin{bmatrix} {}^F T_M \end{bmatrix} = \begin{bmatrix} {}^N A_F \end{bmatrix} {}^F \begin{bmatrix} {}^F T_M \end{bmatrix} \begin{bmatrix} {}^N A_F \end{bmatrix}^{-1} \quad 2.11$$

Thus, twists created in different reference frames can all be expressed in a common frame of reference. For instance, in a serial chain, the total twist of the end-effector may be considered as a linear combination of various twist contributions expressed in a common frame. For example:

$${}^M \begin{bmatrix} {}^F T_M \end{bmatrix} = \underbrace{\begin{bmatrix} {}^M A_1 \end{bmatrix}^{-1} \begin{bmatrix} {}^F T_1 \end{bmatrix} \begin{bmatrix} {}^M A_1 \end{bmatrix}}_{T_1} + \underbrace{\begin{bmatrix} {}^M A_2 \end{bmatrix}^{-2} \begin{bmatrix} {}^2 T_M \end{bmatrix} \begin{bmatrix} {}^M A_2 \end{bmatrix}^{-1}}_{T_2} + \dots + \underbrace{{}^M \begin{bmatrix} {}^N T_M \end{bmatrix}}_{T_N} \quad 2.12$$

Such twist matrices can be rewritten as linear combinations of twist vectors parameterized by the corresponding manipulation variable rates $\vec{v} = [v_1 \ v_2 \ \dots \ v_N]^T$ (For instance, $\dot{\theta}$ for revolute joint). A geometrically assembled Jacobian matrix (J) may now be written as:

$${}^M [{}^F t_M] = \underbrace{[\vec{t}_1 \ \vec{t}_2 \ \dots \ \vec{t}_N]}_J \begin{bmatrix} v_1 \\ v_2 \\ \vdots \\ v_N \end{bmatrix} \quad 2.13$$

Above material of the homogeneous transformations and related group theory is discussed in greater details in (Murray, Li and Sastry, 1993).

Two-link Manipulator Kinematics

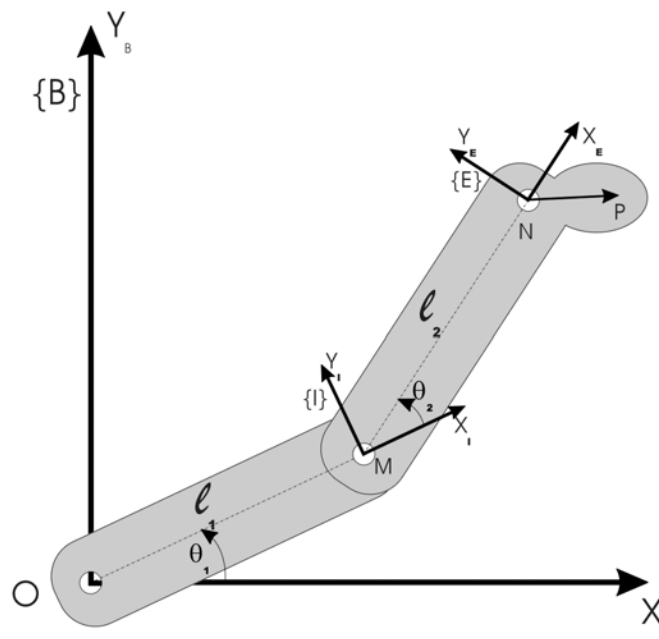


FIGURE 2-2: TWO LINK MANIPULATOR

Consider a two-link planar manipulator as shown in Figure 2-2. The fixed base frame is denoted by $\{B\}$, an intermediate frame is denoted by $\{I\}$ and the end-effector frame is denoted by $\{E\}$. Note that there could be more than one intermediate links and so more than one intermediate frames. Let $\vec{p} = [x_E, y_E]^T$ denote the location of end effector and $\vec{q} = [\theta_1, \theta_2]^T$ be the configuration vector. l_1 and l_2 are the link lengths of the manipulator. We next show two different approaches to model the position and velocity kinematics of such a manipulator.

Traditional Approach

The forward kinematics equations give the relation between the position vector \vec{p} and the configuration vector \vec{q} as:

$$\vec{p} = \begin{bmatrix} x_E \\ y_E \end{bmatrix} = \begin{bmatrix} l_1 \cos \theta_1 + l_2 \cos(\theta_1 + \theta_2) \\ l_1 \sin \theta_1 + l_2 \sin(\theta_1 + \theta_2) \end{bmatrix} \quad 2.14$$

Differentiating Equation 2.14 with respect to time gives

$$\dot{\vec{p}} = \begin{bmatrix} \dot{x}_E \\ \dot{y}_E \end{bmatrix} = \begin{bmatrix} -l_1 \sin \theta_1 - l_2 \sin(\theta_1 + \theta_2) & -l_2 \sin(\theta_1 + \theta_2) \\ l_1 \cos \theta_1 + l_2 \cos(\theta_1 + \theta_2) & l_2 \cos(\theta_1 + \theta_2) \end{bmatrix} \begin{bmatrix} \dot{\theta}_1 \\ \dot{\theta}_2 \end{bmatrix} \quad 2.15$$

where

$$J(\vec{q}) = \begin{bmatrix} -l_1 \sin \theta_1 - l_2 \sin(\theta_1 + \theta_2) & -l_2 \sin(\theta_1 + \theta_2) \\ l_1 \cos \theta_1 + l_2 \cos(\theta_1 + \theta_2) & l_2 \cos(\theta_1 + \theta_2) \end{bmatrix} \quad 2.16$$

J is a Jacobian matrix, matrix that maps the joint rates into the Cartesian velocities (Angeles, 2002). Note that, while the position kinematics is a nonlinear

relation, the corresponding velocity kinematics is linear and can be expressed in matrix form.

Twist Based Approach

Considering the frames $\{B\}$, $\{I\}$ and $\{E\}$ as shown in Figure 2-2, the homogeneous transform ${}^B A_E$ that transforms a vector in frame $\{E\}$ to a vector in frame $\{B\}$ can be written as:

$${}^B A_E = {}^B A_I {}^I A_E = \begin{bmatrix} \cos(\theta_1 + \theta_2) & -\sin(\theta_1 + \theta_2) & x_E \\ \sin(\theta_1 + \theta_2) & \cos(\theta_1 + \theta_2) & y_E \\ 0 & 0 & 1 \end{bmatrix} \quad 2.17$$

where ${}^B A_E$, ${}^B A_I$ and ${}^I A_E \in SE(2)$.

Differentiating Equation 2.17 with respect to time and pre-multiplying by its inverse to obtain body twist gives

$${}^E [{}^B T_E] = [{}^B A_E]^{-1} {}^B \dot{A}_E = [{}^B A_E]^{-1} {}^B \dot{A}_I {}^I A_E + [{}^I A_E]^{-1} {}^I \dot{A}_E \quad 2.18$$

A body-fixed twist based Jacobian can be constructed by extracting corresponding body twist vectors from the twist matrix and written as:

$$J = \begin{bmatrix} 1 & 1 \\ l_1 \sin \theta_2 & 0 \\ l_2 + l_1 \cos \theta_2 & l_2 \end{bmatrix} \quad 2.19$$

Following a similar process, a spatial twist based Jacobian matrix can be constructed from the spatial twists and can be given by:

$$J = \begin{bmatrix} 1 & 1 \\ 0 & l_1 \sin \theta_1 \\ 0 & -l_1 \cos \theta_1 \end{bmatrix} \quad 2.20$$

Jacobian Based Performance Measures

Performance measures and metrics play a critical role in quantitatively capturing desirable qualitative performance characteristics and find application in all aspects of manipulator design, control and ultimately evaluation of system performance.

Manipulability based performance indices have played a significant role in quantitatively evaluate robotic manipulators along with other metrics like size of workplace, positioning accuracy, load carrying capacity, speed, reliability, cost, ease of operation and settling time. As Jacobian based measures, such manipulability indices have served both as a measure of end-effector motion/force capabilities as well as of the motion/force transmissibility of the manipulator and various authors emphasize specific aspects. For instance, (Park and Kim, 1998), define manipulability as “the ability to move and apply forces in arbitrary directions,” whereas (Bicchi and Prattichizza, 2000) define it as “the directions in the task or joint space that extremize the ratio between some measure of effort in the joint space and a measure of performance in task space”. (Park and Kim, 1996) also present a coordinate invariant differential geometric analysis of manipulability of holonomic closed loop chains.

In our work however, we focus only on using kinematic manipulability in evaluating the manipulator performance in various relative configurations.

Some of these kinematic manipulability concepts are explained with the aid of Singular Value Decomposition (SVD) (Nakamura, 1991) of the Jacobian matrix and affiliated concepts. Considering the Jacobian of a manipulator that maps joint rates into corresponding task space velocities, SVD of the Jacobian matrix yields,

$$J = U\Sigma V^T \quad 2.21$$

where U is a $m \times m$ orthonormal rotation matrix, V is a $n \times n$ orthonormal rotation matrix and Σ is $m \times n$ matrix that can be expressed as:

$$\Sigma = \text{diag}(\sigma_1, \sigma_2, \dots, \sigma_k, 0, \dots, 0)_{m \times n} \quad 2.22$$

$$\begin{aligned} \sigma_1 &\geq \sigma_2 \geq \dots \geq \sigma_k \\ k &= \text{rank}(J) \end{aligned} \quad 2.23$$

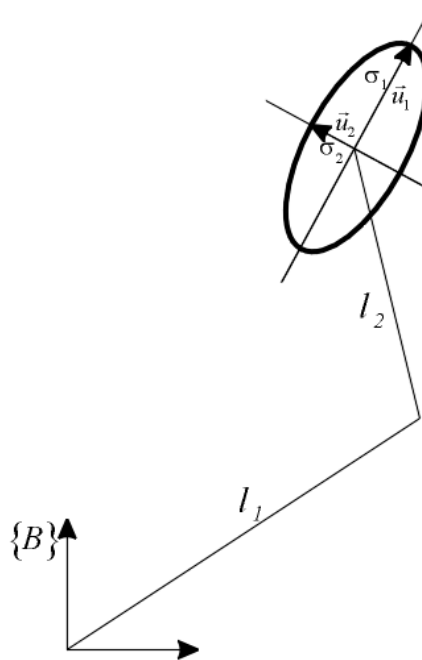


FIGURE 2-3: MANIPULABILITY ELLIPSOID FOR A TWO LINK PLANAR MANIPULATOR

The value of k in Equation 2.23 is the rank of matrix J which should always be less than or equal to minimum of m and n . The effect of the linear mapping by the Jacobian can also be interpreted (and visualized) geometrically using the notation of a manipulability ellipsoid. The Jacobian is assumed to map unit sphere in the joint space into a corresponding ellipsoid in the task space. The columns of the U matrix, $\vec{u}_1, \vec{u}_2, \dots, \vec{u}_k$, can now be interpreted as the directions of principal axis and the singular values, $\sigma_1, \sigma_2, \dots, \sigma_k$, can be interpreted as the corresponding magnitudes of principal axis. Thus, principal axis are given by $\vec{u}_1\sigma_1, \vec{u}_2\sigma_2, \dots, \vec{u}_k\sigma_k$. The major axis of this ellipsoid $\vec{u}_1\sigma_1$ corresponds to the direction in which the end-effector can move most easily and least easily in the minor axis $\vec{u}_k\sigma_k$ direction. When this ellipsoid becomes a sphere, the end-effector can move with uniform ease in all directions. Such SVD and the subsequent geometric interpretation as a manipulability ellipsoid permits a very useful interpretation of various measures of manipulability defined in the literature and will be summarized next.

Yoshikawa's Measure of Manipulability (MOM)

$$\Gamma_y = \sigma_1\sigma_2\dots\sigma_k \quad 2.24$$

(Yoshikawa, 1985) first defined manipulability as $\Gamma_y = \sqrt{\det(JJ^T)}$ which in the context of the SVD may now be interpreted as the product of the singular values of the Jacobian matrix. Geometrically, this product of the singular values is directly proportional to the volume of the ellipsoid. However, this measure cannot distinguish

between large but narrow ellipsoids and small but more uniformly spherical ellipsoids and hence, we avoid its use.

Condition Number

$$\Gamma_c = \frac{\sigma_1}{\sigma_k} \quad 2.25$$

(Salisbury and Craig, 1982) used the condition number as a design tool as it quantifies the error in the positioning of the end-effector induced because of error in controlling the joints to their set-points. Geometrically it is the ratio of the major and minor axes of the manipulability ellipsoid. However, near singular configurations, the metric grows out of bounds and approaches infinity.

Isotropy Index

$$\Gamma_i = \frac{\sigma_k}{\sigma_1} \quad 2.26$$

(Angeles, 1991) used this measure of manipulability as a global performance index. Geometrically this measure expressed as the ratio of minor to major axis also relates their relative sizes. However, as it is better behaved than the condition number since it always remains bounded between 0 and 1 and is the preferred measure of manipulability in our work.

Riemannian Metrics Based Performance Measures

In this section, we follow the treatment of Riemannian metrics principally from Zefran (1996). In order to evaluate performance of a configuration, a suitable metric defined on $SE(3)$ space is required. Because $SE(3)$ (the space of all positions and orientations) is not Euclidean, there is no obvious choice of a metric on this set. An inner

product on $se(3)$ can be extended to a Riemannian metric on $SE(3)$. Let the inner product of two elements $T_1, T_2 \in se(3)$ be given by

$$\langle T_1, T_2 \rangle_I = \vec{t}_1^T W \vec{t}_2 \quad 2.27$$

where \vec{t}_1 and \vec{t}_2 are 3×1 vectors of components of T_1 and T_2 with respect to some basis and W is a positive definite matrix. If \vec{V}_1 and \vec{V}_2 are tangent vectors at an arbitrary point $A \in SE(3)$, the inner product $\langle \vec{V}_1, \vec{V}_2 \rangle_A$ in the tangent space $T_A SE(3)$ can be defined by:

$$\langle \vec{V}_1, \vec{V}_2 \rangle_A = \langle A^{-1} \vec{V}_1, A^{-1} \vec{V}_2 \rangle_I \quad 2.28$$

The metric obtained in such a way is called left invariant metric. A left invariant metric means that it does not depend on the choice of inertial frame. However, it definitely depends on the choice of body fixed frame. There does not exist a bi-invariant metric on $SE(3)$.

A family of left-invariant metrics on $se(3)$, parameterized by three scalars α , β and γ , can be expressed as:

$$W = \begin{bmatrix} \alpha I_{3 \times 3} & \beta I_{3 \times 3} \\ \beta I_{3 \times 3} & \gamma I_{3 \times 3} \end{bmatrix} \quad 2.29$$

Several left invariant metrics can be found in literature by using different values for α , β and γ . For example, $\beta = \gamma = 0$ is called Killing form which essentially is a measure of the angular velocities ($\alpha \vec{\omega}^T \vec{\omega}$) within the space of twists. $\alpha = \gamma = 0$ results in the Klein form and serves as a measure of $(2 \vec{\omega}^T \vec{v})$. (However, when specialized to

$SE(2)$, this measure is identically zero and we avoid its use). $\beta = 0$ yields the decoupled Park metric which serves as a weighted quadratic combination of the linear and angular velocities $\alpha(\vec{\omega}^T \vec{\omega}) + \gamma(\vec{v}^T \vec{v})$. Similarly, in the centroid fixed frame of reference aligned along the principal inertial directions, the kinetic energy metric can be written as:

$$W = \begin{bmatrix} H_{3 \times 3} & \mathbf{0}_{3 \times 3} \\ \mathbf{0}_{3 \times 3} & mI_{3 \times 3} \end{bmatrix} \quad 2.30$$

The metrics shown in Equation 2.29 can be specialized for $SE(2)$, and written as:

$$W = \begin{bmatrix} \alpha_{1 \times 1} & \mathbf{0}_{1 \times 2} \\ \mathbf{0}_{2 \times 1} & \gamma I_{2 \times 2} \end{bmatrix} \quad 2.31$$

and similarly the metric shown in Equation 2.30 may be specialized as:

$$W = \begin{bmatrix} I_{zz} & \mathbf{0}_{1 \times 2} \\ \mathbf{0}_{2 \times 1} & mI_{2 \times 2} \end{bmatrix} \quad 2.32$$

where m and I_{zz} are the mass and planar inertia of the rigid body.

Curve Representation and Geometric Invariants

A curve is defined as a continuous map from one dimensional space to an n dimensional space. In a Cartesian coordinate system, let

$$x = x(t), y = y(t) \quad 2.33$$

be continuous functions of a real parameter t over a closed interval $[t_1, t_2]$ (i.e., $[t_1 \leq t \leq t_2]$). The points $P(t) \equiv (x(t), y(t))$ for $[t_1 \leq t \leq t_2]$ are said to constitute a planar curve joining the endpoints $P(t_1)$ and $P(t_2)$. The specification of a curve in terms of one

or more parameters which can take on values in a specified range as given in Equation 2.33 is called a parameterization of the curve. While any suitable monotonically increasing variable such as time, arc-length, number of points on curve or index number could serve as a suitable parameter, an arc-length parameterization being geometric invariant, is the preferred parameterization.

An arbitrary parameterization $P(t) \equiv (x(t), y(t))$ can be converted to a suitable arc-length parameterization $P(s) \equiv (x(s), y(s))$ by considering a mapping $\Phi: s \rightarrow t$ such that $t = \Phi(s)$. Thus, $P(t) \equiv (x(t), y(t)) = (x(\Phi(s)), y(\Phi(s))) = (x(s), y(s))$ is an arc-length parametric curve.

Serret-Frenet Frame

Given an arc-length parameterized path in $\mathbb{R}^2(x(s), y(s))$, a unit tangent vector \hat{e}_t can be computed for any point on curve, by taking derivative of the curve with respect to the parameter s . A unit normal vector can then be computed such that it satisfies the relation given in Equation 2.34.

$$\hat{e}_t(s) \cdot \hat{e}_n(s) = 0 \tag{2.34}$$

Taking derivative of this equation,

$$\dot{\hat{e}}_t(s) \cdot \hat{e}_n(s) + \hat{e}_t(s) \cdot \dot{\hat{e}}_n(s) = 0 \tag{2.35}$$

For some suitable constant $\kappa(s)$,

$$\begin{bmatrix} \dot{\hat{e}}_t(s) \\ \dot{\hat{e}}_n(s) \end{bmatrix} = \begin{bmatrix} 0 & \kappa(s) \\ -\kappa(s) & 0 \end{bmatrix} \begin{bmatrix} \hat{e}_t(s) \\ \hat{e}_n(s) \end{bmatrix} \quad 2.36$$

satisfies the derivative equation. Equation 2.36 is a set of vector differential equations known as Serret-Frenet formula. $\kappa(s)$ is called the curvature of the curve. When $\kappa(s)$ is constantly zero, \hat{e}_t never changes and the curve is a straight line. $\kappa(s)$ thus, measures the rate at which any non-straight curve tends to depart from its tangent. Thus, Serret-Frenet formulas relate inherent properties of a parameterized curve. A frame can now be attached in such a way that x axis of the frame is coincident with \hat{e}_t and y axis with \hat{e}_n . This frame is known as Serret-Frenet frame.

However, in many cases, we may not have a continuous curve, but just a set of discrete data points. This may especially occur when we record external world data with the help of a digital computer, or when we are given a set of data points through which the curve should pass. In such cases, we generate cubic interpolating splines from the available data.

Cubic Interpolating Splines

A spline is defined as a polynomial function having simple local form yet flexible and smooth globally. A cubic spline is a spline constructed out of piecewise third-order polynomials which passes through a set of $n+1$ control points. The second derivative of each polynomial is commonly set to zero at the endpoints, since this provides a boundary condition that completes the system of $n-1$ equations. This produces a "natural" cubic spline and leads to a tridiagonal system which can be solved to give the coefficients of the polynomials. However, this choice is not the only one possible; other boundary

bold line joining all the points from P_1 to P_5 . Hence the accuracy of the arc-length depends on the “suitable” number of segments in which the curve is divided.

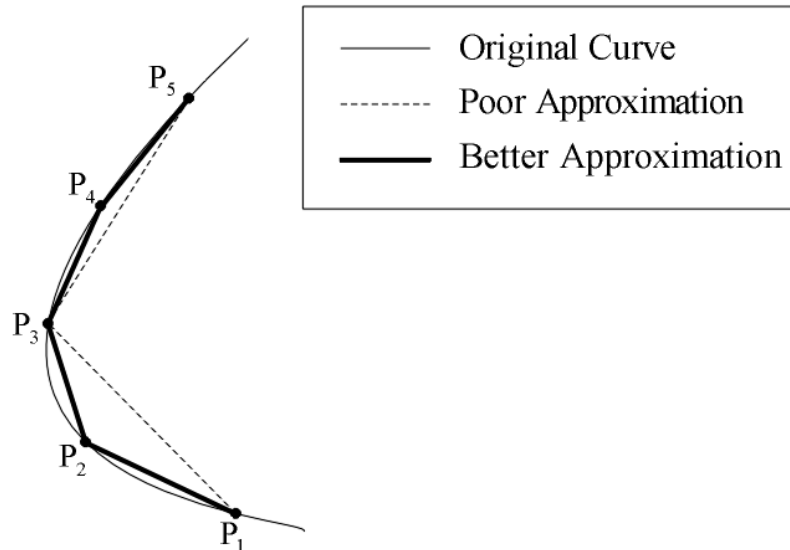


FIGURE 2-4: ARC-LENGTH AS A FUNCTION OF NUMBER OF SEGMENTS

The approach taken in this work is to iteratively divide the curve in an increasing number of segments starting with a lower number, until the difference between the arc-length calculated in preceding iteration and current iteration is less than certain error value. This approach works yields an approximation that is in desired limits regardless of the scale or inherent geometry of the curve.

Computation of Frenet-Serret Coefficients for the Cubic Spline Approximation:

The curvature of a curve at any point is the arc-rate of rotation of the tangent. Hence, it is useful to reparameterize a given curve in terms of arc-length. Assume that we are given the parametric equation of a plane curve $x = x(t)$ and $y = y(t)$. For a general curve, the variance in t is not directly related to the distance along the curve. By reparameterizing the curve in terms of arc-length s , the parameter itself now gives the

distance traveled along the curve. Curvature can now be defined as the rate of change of tangential angle φ with respect to arc length s .

$$\kappa(s) = \frac{d\varphi}{ds} \quad 2.40$$

It is sometimes possible to come up with an algebraic expression for the arc-length of a curve for many standard curves. However, in general, the curve must be parameterized numerically.

For the given plane curve $x = x(t)$ and $y = y(t)$, the first and second derivatives of x and y can be calculated. If the curve is a cubic spline, i.e.

$$\begin{aligned} x(t) &= a_x + b_x t + c_x t^2 + d_x t^3 \\ y(t) &= a_y + b_y t + c_y t^2 + d_y t^3 \end{aligned} \quad 2.41$$

Taking the first derivative of above equation with respect to parameter t gives

$$\begin{aligned} x'(t) &= \frac{dx}{dt} = b_x + 2c_x t + 3d_x t^2 \\ y'(t) &= \frac{dy}{dt} = b_y + 2c_y t + 3d_y t^2 \end{aligned} \quad 2.42$$

and taking second derivate gives

$$\begin{aligned} x''(t) &= \frac{dx'}{dt} = 2c_x + 6d_x t \\ y''(t) &= \frac{dy'}{dt} = 2c_y + 6d_y t \end{aligned} \quad 2.43$$

Now the value of curvature κ can be calculated as:

$$\kappa = \frac{x'y'' - y'x''}{(x'^2 + y'^2)^{3/2}} \quad 2.44$$

For greater details into the theory of curves, reader is encouraged to read references (Coxeter, 1969; Wolfram).

Chapter 3

Mobile Manipulators

In this chapter, we develop the terminology and notation to model the individual Wheeled Mobile Robot (WMR), the Mobile Manipulator (MM) and the virtual structure that are used in subsequent work. In all of the subsequent modeling we assume a planar system, i.e. the WMR and mounted manipulator move in planes parallel to the ground plane.

Wheeled Mobile Robot

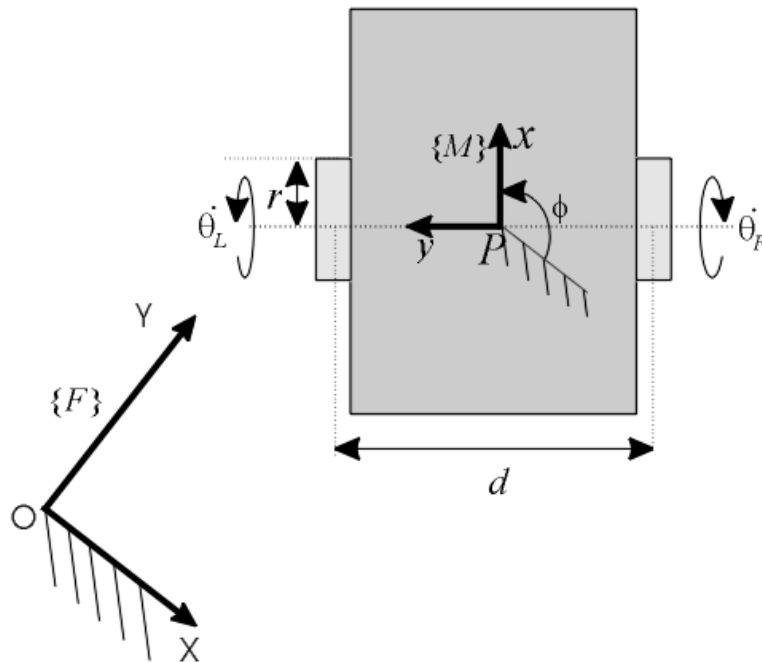


FIGURE 3-1: A WHEELED MOBILE ROBOT

Consider a differentially-driven nonholonomic WMR moving in a plane. A body fixed frame $\{M\}$ is attached to this mobile robot at the center of the axle P with the x

axis pointing in the forward direction of travel as shown in Figure 3-1. Let ϕ be the angle that frame $\{M\}$ makes with an inertial frame $\{F\}$. We now look at two different approaches to model a WMR.

Traditional Configuration Modeling

The configuration of the WMR can be locally parameterized by a configuration vector $\vec{q} = [x \ y \ \phi]^T$. This mobile base is subjected to a nonholonomic constraint that can be written as:

$$\dot{x} \sin \phi - \dot{y} \cos \phi = 0 \quad 3.1$$

or in Pfaffian form as:

$$A(\vec{q})\dot{\vec{q}} = 0 \quad 3.2$$

where $A(\vec{q}) = [\sin \phi \ -\cos \phi \ 0]$. The set of feasible configuration velocities $\dot{\vec{q}} = [\dot{x} \ \dot{y} \ \dot{\phi}]^T$ that are consistent with this nonholonomic constraint can thus be determined to lie in the null space of this constraint matrix. Let $S(\vec{q})$ be a matrix whose columns span the null space of A . i.e. $A(\vec{q})S(\vec{q}) = 0$. While the choice of $S(\vec{q})$ is non-unique, one commonly parameterization of the feasible configuration velocities is given by:

$$\dot{\vec{q}} = \begin{bmatrix} \dot{x} \\ \dot{y} \\ \dot{\phi} \end{bmatrix} = \begin{bmatrix} \cos \phi & 0 \\ \sin \phi & 0 \\ 0 & 1 \end{bmatrix} \begin{bmatrix} {}^M\vec{v} \\ {}^M\vec{\omega} \end{bmatrix} \quad 3.3$$

where ${}^M\vec{v}$ and ${}^M\vec{\omega}$ are the forward translational velocity and angular velocity of the WMR expressed in body fixed frame $\{M\}$. Alternately, the feasible configuration velocities may also be expressed in terms of angular velocities at each wheel. Let r be the radius of wheels of this mobile robot and d be the distance between the two wheels as shown in Figure 3-1. Assuming that the left and right wheels rotate with angular velocities $\dot{\theta}_L$ and $\dot{\theta}_R$ about the axis parallel to axle, the forward translational velocity and angular velocity can be written in frame $\{M\}$ as:

$$\begin{aligned} {}^M\vec{v}_x &= r \left(\frac{\dot{\theta}_L + \dot{\theta}_R}{2} \right) \\ {}^M\dot{\phi} &= r \left(\frac{\dot{\theta}_R - \dot{\theta}_L}{d} \right) \end{aligned} \tag{3.4}$$

or in matrix form as

$$\begin{bmatrix} {}^M\vec{v} \\ {}^M\dot{\phi} \end{bmatrix} = \begin{bmatrix} \frac{r}{2} & \frac{r}{2} \\ -\frac{r}{d} & \frac{r}{d} \end{bmatrix} \begin{bmatrix} \dot{\theta}_L \\ \dot{\theta}_R \end{bmatrix} \tag{3.5}$$

By substituting Equation 3.5 into Equation 3.3, the configuration vector velocities can now be expressed in terms of the wheel velocities as

$$\dot{\vec{q}} = \begin{bmatrix} \frac{r}{2} \cos \phi & \frac{r}{2} \cos \phi \\ \frac{r}{2} \sin \phi & \frac{r}{2} \sin \phi \\ -\frac{r}{d} & \frac{r}{d} \end{bmatrix} \begin{bmatrix} \dot{\theta}_L \\ \dot{\theta}_R \end{bmatrix} \tag{3.6}$$

Alternate Configuration Modeling

An alternate configuration modeling is also possible using homogeneous transforms, twist matrix and twist vector notation and is detailed below. The configuration vector of this wheeled mobile base can also be given by the homogeneous transform ${}^F A_M = ({}^F R_M, {}^F \vec{p}) \in SE(2)$, where

$${}^F R_M = \begin{bmatrix} \cos \phi & -\sin \phi \\ \sin \phi & \cos \phi \end{bmatrix} \in SO(2) \quad 3.7$$

$${}^F \vec{p} = [x \quad y]^T \in \mathbb{R}^2 \quad 3.8$$

where ${}^F R_M$ is a rotation matrix denoting the relative orientation of frame $\{M\}$ with respect to $\{F\}$ and ${}^F \vec{p}$ denotes the relative displacement. The relative twist matrix of this mobile robot as expressed in mobile base frame is:

$${}^M [{}^F T_M] = \begin{bmatrix} 0 & 0 & \dot{x} \cos \phi + \dot{y} \sin \phi \\ 0 & 0 & -\dot{x} \sin \phi + \dot{y} \cos \phi \\ 0 & 0 & 0 \end{bmatrix} + \begin{bmatrix} 0 & -\dot{\phi} & 0 \\ \dot{\phi} & 0 & 0 \\ 0 & 0 & 0 \end{bmatrix} \quad 3.9$$

where the term $-\dot{x} \sin \phi + \dot{y} \cos \phi$ represents the velocity of the mobile base in the direction parallel to y_M axis of frame $\{M\}$ expressed in $\{M\}$.

Since the mobile base must satisfy nonholonomic constraints as given by Equation 3.1, $-\dot{x} \sin \phi + \dot{y} \cos \phi$ must be identically zero. Noting that the forward translational velocity of the mobile base, ${}^M \vec{v} = \dot{x} \cos \phi + \dot{y} \sin \phi$ Equation 3.9 can be written as:

$${}^M \begin{bmatrix} F T_M \end{bmatrix} = \begin{bmatrix} 0 & 0 & {}^M \vec{v} \\ 0 & 0 & 0 \\ 0 & 0 & 0 \end{bmatrix} + \begin{bmatrix} 0 & -\dot{\phi} & 0 \\ \dot{\phi} & 0 & 0 \\ 0 & 0 & 0 \end{bmatrix} \quad 3.10$$

A Jacobian matrix can be assembled by extracting corresponding twist vectors from Equation 3.10 as:

$${}^M \begin{bmatrix} F t_M \end{bmatrix} = \begin{bmatrix} 1 & 0 \\ 0 & 0 \\ 0 & 1 \end{bmatrix} \begin{bmatrix} {}^M \vec{v} \\ {}^M \dot{\phi} \end{bmatrix} \quad 3.11$$

Substituting the Equation 3.5, the total twist based Jacobian matrix can be determined to be

$${}^M \begin{bmatrix} F t_M \end{bmatrix} = \begin{bmatrix} \frac{r}{2} & \frac{r}{2} \\ 0 & 0 \\ -\frac{r}{d} & \frac{r}{d} \end{bmatrix} \begin{bmatrix} \dot{\theta}_L \\ \dot{\theta}_R \end{bmatrix} \quad 3.12$$

Mobile Manipulator

A MM is a WMR with a multilink manipulator mounted on it. shows a MM with three links maneuvering in a plane with fixed frame $\{F\}$. Base frame $\{B\}$ on mobile robot, intermediate frames $\{I_1\}$ and $\{I_2\}$ on the distal ends of link-1 and link-2 respectively and end-effector frame $\{E\}$ on the distal end of link-3, are assigned following the Denavit-Hartenberg (Denavit and Hartenberg, 1955) convention. Let l_1 , l_2 and l_3 be the lengths of the three links and θ_1 , θ_2 and θ_3 be the relative angles between frames $\{B\}$ and $\{I_1\}$, $\{I_1\}$ and $\{I_2\}$ and $\{I_2\}$ and $\{E\}$ respectively, measured in the counter-clockwise direction. The configuration vector of this MM is then given by

$g = ({}^F R_M, {}^F \vec{p}, \theta_1, \theta_2, \theta_3) \in SE(2) \times T^3$ Let the base frame $\{B\}$ be located at a constant offset (a, b) from frame $\{M\}$. Let r be the radius of the wheels and d be the distance between two wheels. Note that the link-3 can be considered a part of the object to be transported in such a way that the end-effector frame $\{E\}$ makes a constant offset with the frame of the object.

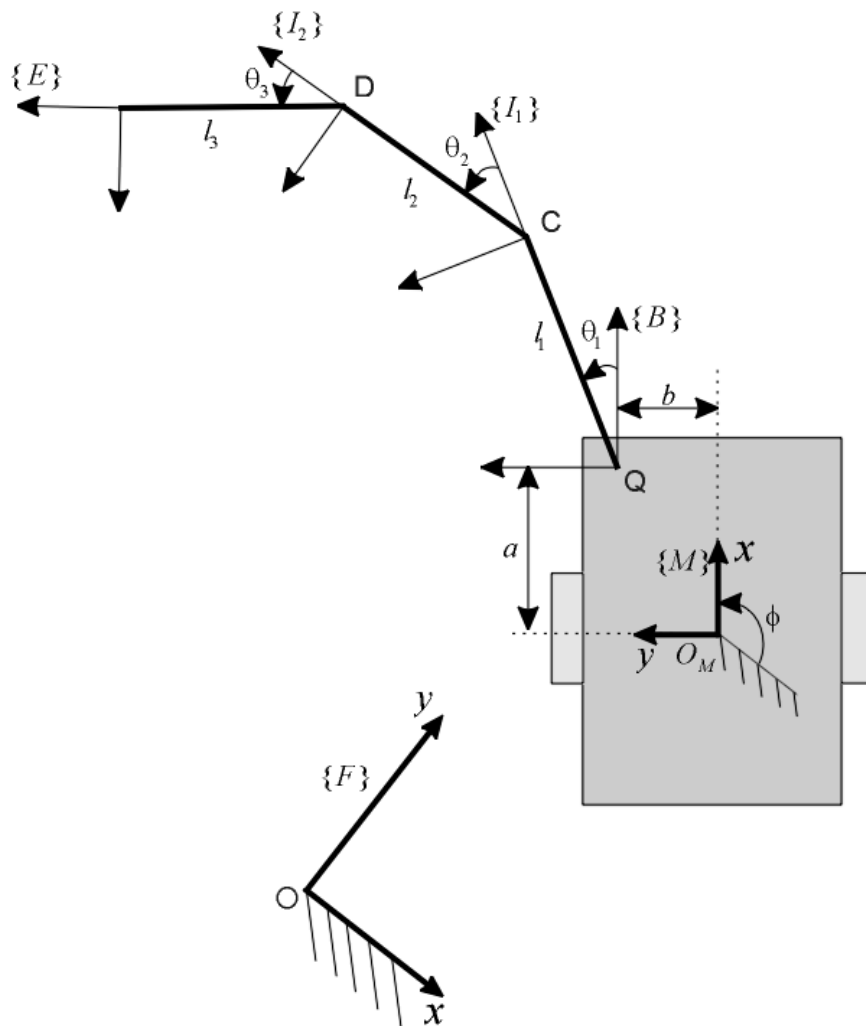


FIGURE 3-2: A MOBILE MANIPULATOR

The homogeneous transform that transforms a vector quantity in frame $\{E\}$ to a vector quantity in frame $\{F\}$ is written as:

$${}^F A_E = {}^F A_M {}^M A_B {}^B A_{I_1} {}^{I_1} A_{I_2} {}^{I_2} A_E \quad 3.13$$

If the location of origin O_M of MM frame $\{M\}$ is (x, y) , then from , we get:

$${}^F A_M = \begin{bmatrix} \cos \phi & -\sin \phi & x \\ \sin \phi & \cos \phi & y \\ 0 & 0 & 1 \end{bmatrix} \quad 3.14$$

Similarly,

$${}^M A_B = \begin{bmatrix} 1 & 0 & a \\ 0 & 1 & b \\ 0 & 0 & 1 \end{bmatrix} \quad 3.15$$

$${}^B A_{I_1} = \begin{bmatrix} \cos \theta_1 & -\sin \theta_1 & l_1 \cos \theta_1 \\ \sin \theta_1 & \cos \theta_1 & l_1 \sin \theta_1 \\ 0 & 0 & 1 \end{bmatrix} \quad 3.16$$

$${}^{I_1} A_{I_2} = \begin{bmatrix} \cos \theta_2 & -\sin \theta_2 & l_2 \cos \theta_2 \\ \sin \theta_2 & \cos \theta_2 & l_2 \sin \theta_2 \\ 0 & 0 & 1 \end{bmatrix} \quad 3.17$$

$${}^{I_2} A_E = \begin{bmatrix} \cos \theta_3 & -\sin \theta_3 & l_3 \cos \theta_3 \\ \sin \theta_3 & \cos \theta_3 & l_3 \sin \theta_3 \\ 0 & 0 & 1 \end{bmatrix} \quad 3.18$$

Differentiating Equation 3.13 with respect to time and pre-multiplying it by

$$\begin{aligned} & \left[{}^F A_E \right]^{-1}, \\ & \underbrace{\left[{}^F A_E \right]^{-1} F \dot{A}_E}_{E[{}^F T_E]} = \underbrace{\left[{}^M A_E \right]^{-1} \left[{}^F A_M \right]^{-1} F \dot{A}_M}_{M[{}^F T_M]} {}^M A_E + \underbrace{\left[{}^B A_E \right]^{-1} \left[{}^M A_B \right]^{-1} M \dot{A}_B}_{B[{}^M T_B]} {}^B A_E \\ & \quad + \underbrace{\left[{}^{I_1} A_E \right]^{-1} \left[{}^B A_{I_1} \right]^{-1} B \dot{A}_{I_1}}_{I_1[{}^B T_{I_1}]} {}^{I_1} A_E + \underbrace{\left[{}^{I_2} A_E \right]^{-1} \left[{}^{I_1} A_{I_2} \right]^{-1} I_1 \dot{A}_{I_2}}_{I_2[{}^{I_1} T_{I_2}]} {}^{I_2} A_E + \underbrace{\left[{}^{I_2} A_E \right]^{-1} I_2 \dot{A}_E}_{E[{}^{I_2} T_E]} \end{aligned} \quad 3.19$$

where ${}^E [{}^F T_E]$ is the body fixed twist matrix. The components $\bar{\omega}$ and \bar{v} of the corresponding body fixed twist vector ${}^E [{}^F t_E]$ represents the angular velocity and linear velocity of origin O_E of the end-effector frame $\{E\}$ as expressed in frame $\{E\}$. Note that ${}^M A_B = \text{constant}$ and thus, ${}^M \dot{A}_B = {}^B [{}^M T_B] = 0$. We can write the twist matrix ${}^M [{}^F T_M]$ from Equation 3.12 as

$${}^M [{}^F T_M] = \begin{bmatrix} 0 & \frac{r}{d} \dot{\theta}_L & \frac{r}{2} \dot{\theta}_L \\ -\frac{r}{d} \dot{\theta}_L & 0 & 0 \\ 0 & 0 & 0 \end{bmatrix} + \begin{bmatrix} 0 & -\frac{r}{d} \dot{\theta}_R & \frac{r}{2} \dot{\theta}_R \\ \frac{r}{d} \dot{\theta}_R & 0 & 0 \\ 0 & 0 & 0 \end{bmatrix} \quad 3.20$$

Expressing all quantities in the end-effector frame $\{E\}$,

$${}^E [{}^F T_M] = [{}^M A_E]^{-1} {}^M [{}^F T_M] {}^M A_E = \begin{bmatrix} 0 & -\frac{\dot{\theta}_L}{2r} & C_1 \dot{\theta}_L \\ \frac{\dot{\theta}_L}{2r} & 0 & C_2 \dot{\theta}_L \\ 0 & 0 & 0 \end{bmatrix} + \begin{bmatrix} 0 & -\frac{\dot{\theta}_R}{2r} & C_3 \dot{\theta}_R \\ \frac{\dot{\theta}_R}{2r} & 0 & C_4 \dot{\theta}_R \\ 0 & 0 & 0 \end{bmatrix} \quad 3.21$$

where

$$C_1 = \frac{-l_2 r \sin \theta_3 - l_1 r \sin(\theta_2 + \theta_3) - ar \sin \Theta + br \cos \Theta}{d} + \frac{r \sin \Theta - 2a \cos \Theta - 2b \sin \Theta - 2l_1 \cos(\theta_2 + \theta_3) - 2l_2 \cos \theta_3 - 2l_3}{2} \quad 3.22$$

$$C_2 = \frac{-l_3 r - l_2 r \cos \theta_3 - l_1 r \cos(\theta_2 + \theta_3) - ar \cos \Theta - br \sin \Theta}{d} + \frac{r \cos \Theta + 2a \sin \Theta - 2b \cos \Theta + 2l_1 \sin(\theta_2 + \theta_3) + 2l_2 \sin \theta_3}{2} \quad 3.23$$

$$C_3 = \frac{l_2 r \sin \theta_3 + l_1 r \sin(\theta_2 + \theta_3) + ar \sin \Theta - br \cos \Theta}{d} + \frac{r \sin \Theta - 2a \cos \Theta - 2b \sin \Theta - 2l_1 \cos(\theta_2 + \theta_3) - 2l_2 \cos \theta_3 - 2l_3}{2} \quad 3.24$$

$$C_4 = \frac{l_3 r + l_2 r \cos \theta_3 + l_1 r \cos(\theta_2 + \theta_3) + ar \cos \Theta + br \sin \Theta}{d} + \frac{r \cos \Theta + 2a \sin \Theta - 2b \cos \Theta + 2l_1 \sin(\theta_2 + \theta_3) + 2l_2 \sin \theta_3}{2} \quad 3.25$$

and $\Theta = (\theta_1 + \theta_2 + \theta_3)$

$${}^E [{}^B T_{I_1}] = [{}^{I_1} A_E]^{-1} {}^{I_1} [{}^B T_{I_1}] {}^{I_1} A_E = \begin{bmatrix} 0 & -\dot{\theta}_1 & (l_2 \sin \theta_3 + l_1 \sin(\theta_2 + \theta_3)) \dot{\theta}_1 \\ \dot{\theta}_1 & 0 & (l_3 + l_2 \cos \theta_3 + l_1 \cos(\theta_2 + \theta_3)) \dot{\theta}_1 \\ 0 & 0 & 0 \end{bmatrix} \quad 3.26$$

$$[{}^{I_2} A_E]^{-1} {}^{I_2} [{}^{I_1} T_{I_2}] {}^{I_2} A_E = \begin{bmatrix} 0 & -\dot{\theta}_2 & l_2 \dot{\theta}_2 \sin \theta_3 \\ \dot{\theta}_2 & 0 & (l_3 + l_2 \cos \theta_3) \dot{\theta}_2 \\ 0 & 0 & 0 \end{bmatrix} \quad 3.27$$

$${}^E [{}^{I_2} T_E] = \begin{bmatrix} 0 & -\dot{\theta}_3 & 0 \\ \dot{\theta}_3 & 0 & l_3 \dot{\theta}_3 \\ 0 & 0 & 0 \end{bmatrix} \quad 3.28$$

The corresponding twist vectors may be extracted as:

$${}^E t_1 = \begin{bmatrix} C_1 \\ C_2 \\ -\frac{r}{d} \end{bmatrix} \quad 3.29$$

$${}^E t_2 = \begin{bmatrix} C_3 \\ C_4 \\ \frac{r}{d} \end{bmatrix} \quad 3.30$$

$${}^E t_3 = \begin{bmatrix} l_2 \sin \theta_3 + l_1 \sin(\theta_2 + \theta_3) \\ l_3 + l_2 \cos \theta_3 + l_1 \cos(\theta_2 + \theta_3) \\ 1 \end{bmatrix} \quad 3.31$$

$${}^E t_4 = \begin{bmatrix} l_2 \sin \theta_3 \\ l_3 + l_2 \cos \theta_3 \\ 1 \end{bmatrix} \quad 3.32$$

and

$${}^E t_5 = \begin{bmatrix} 0 \\ l_3 \\ 1 \end{bmatrix} \quad 3.33$$

By augmenting the above twist vectors with $\dot{\theta}_1$, $\dot{\theta}_2$ and $\dot{\theta}_3$, we get

$$\begin{bmatrix} {}^E v \\ {}^E \omega \end{bmatrix} = \underbrace{\begin{bmatrix} {}^E t_1 & {}^E t_2 & {}^E t_3 & {}^E t_4 & {}^E t_5 \end{bmatrix}}_J \begin{bmatrix} \dot{\theta}_R \\ \dot{\theta}_L \\ \dot{\theta}_1 \\ \dot{\theta}_2 \\ \dot{\theta}_3 \end{bmatrix} \quad 3.34$$

The Jacobian matrix J could now be used to analyze the formation by performing SVD analysis and calculating manipulability. For a general MM configuration as shown in , we consider specializations/simplifications that result in 3 types of modules.

Type I: RRR Mobile Manipulator

Considering the offset between the manipulator frame $\{M\}$ and the base frame $\{B\}$ to be zero, ie. $a = b = 0$, the manipulator that is obtained is designated as Type I module.

Type II: RR Mobile Manipulator

An RR MM can be realized from Type I module by considering $l_3 = 0$ and is designated as Type II module.

Type III: R Mobile Manipulator

Type R MM is the most restrictive case, realized from Type I module by considering $l_2 = l_3 = 0$ and is designated as Type III module.

Formations

Consider a team of n differentially driven nonholonomic WMRs maneuvering in the plane as shown in . Affix a body-fixed frame $\{M_i\}$ to each WMR at the center of the axle with the x axis aligned in the direction of forward travel. The configuration of each MM is given by $g_i = ({}^F R_{M_i}, {}^F \vec{p}_i) \in SE(2)$ with respect to some inertial frame $\{F\}$. However, the configuration of an i^{th} WMR can also be described using the notion of a virtual structure. Assume that the origins $\{O_i\}$ of all these frames $\{M_i\}$ form the vertices

of a virtual structure. A “team fixed coordinate frame” $\{M_0\}$ can now be affixed at some convenient location on this virtual structure. The configuration of this coordinate frame $\{M_0\}$ is then given by $g_0 = ({}^F R_{M_0}, {}^F \vec{p}_0) \in SE(2)$ with respect to $\{F\}$.

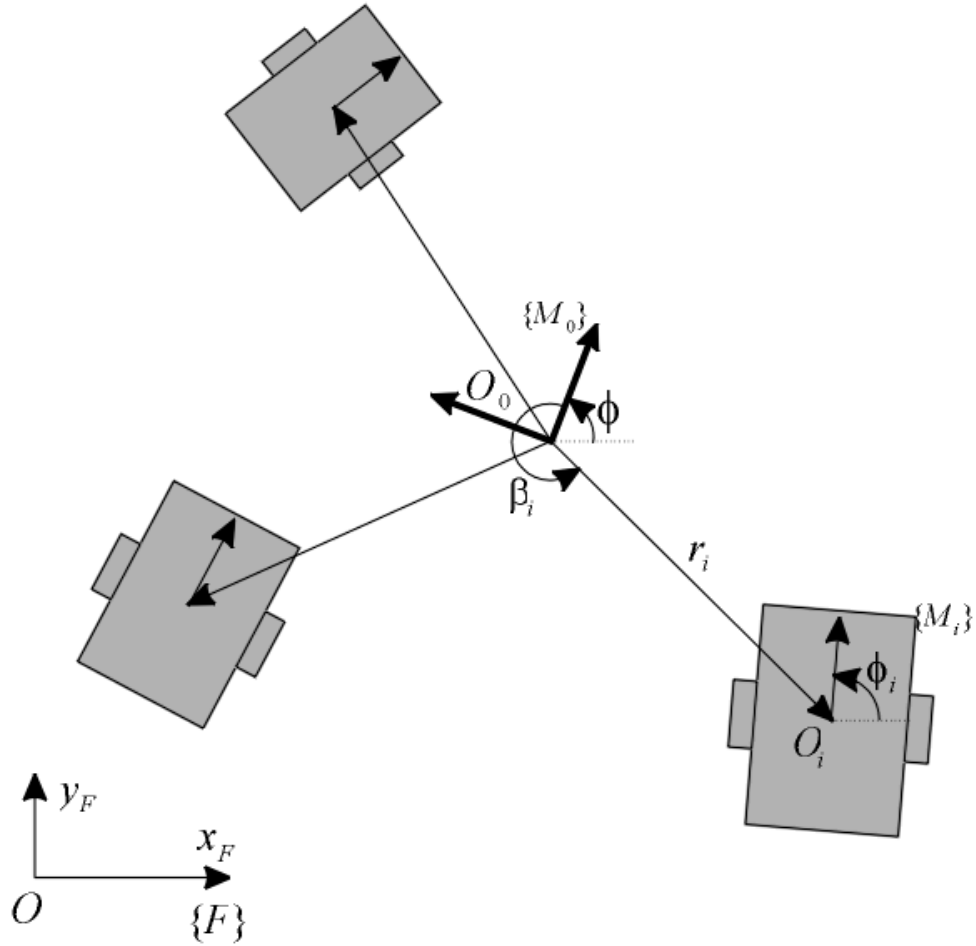


FIGURE 3-3: A FORMATION OF WHEELED MOBILE ROBOTS

A number of approaches have been proposed for selecting the team coordinate frame $\{M_0\}$ with respect to various robot affixed frames $\{M_i\}$. One way is to fix the frame $\{M_0\}$ arbitrarily. The relative orientation of each individual frame $\{M_i\}$ with respect to $\{M_0\}$ can be written as $[{}^F R_{M_0}]^{-1} {}^F R_{M_i}$ and their relative positions by:

$${}^{M_0}\vec{p}_i = \left[{}^F R_{M_0} \right]^{-1} ({}^F \vec{p}_0 - {}^F \vec{p}_i) \in \mathbb{R}^2 \quad 3.35$$

The configuration of the overall formation can thus be written in terms of the configuration of the team-frame (determined by 3 parameters) and $2n$ parameters defining the relative locations of the origins of the individual robots as:

$$q = (g_0, \vec{p}_1, \vec{p}_2, \dots, \vec{p}_n) \in Q = SE(2) \times \underbrace{\mathbb{R}^2 \times \dots \times \mathbb{R}^2}_n \quad 3.36$$

Note that this configuration description eliminates the information regarding the relative orientations of the frame $\{M_i\}$ from the description of the overall formation configuration for reasons discussed later. However, this approach introduces three more configuration parameters in the problem.

An alternate (polar) parameterization of the shape space of the formation is also possible using r_i and β_i . The configuration vector q is then given by

$$q = (g_0, \vec{r}, \vec{\beta}) \in Q = SE(2) \times \mathbb{R}^n \times T^n \quad 3.37$$

where

$$r_i = \left\| {}^{M_0}\vec{p}_i \right\| \quad \text{and} \quad \beta_i = \angle {}^{M_0}\vec{p}_i \quad 3.38$$

(Olfati-Saber and Murray, 2002) proposed a scheme to select the frame $\{M_0\}$ such that it creates a minimal configuration description of the relative formation. Consider a formation given in where each dot denotes a WMR. Affix the frame $\{M_0\}$ at the point O_1 on the first WMR. The orientation of frame $\{M_0\}$ can be determined by aligning x axis in the direction of nearest neighbor O_2 and is denoted as $\{{}^F R_{M_0}\}$. Thus,

the complete system can now be described by 3 parameters for team frame and $2n - 3$ shape parameters describing the relative formation.

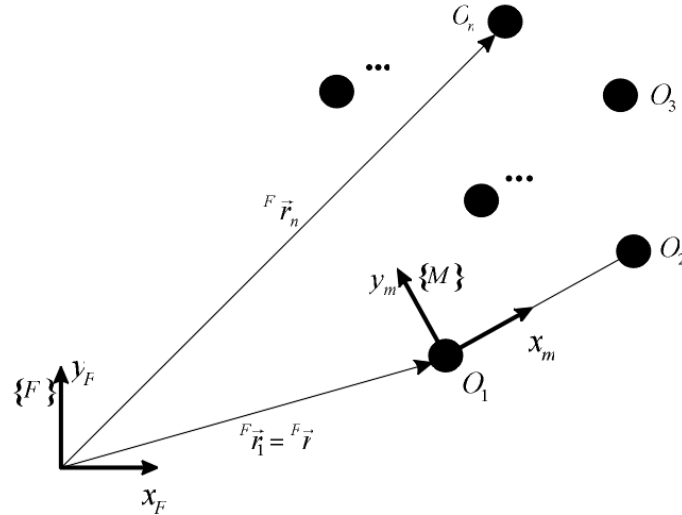


FIGURE 3-4: A FORMATION OF MOBILE ROBOTS

In yet another approach, proposed by (Belta and Kumar, 2002), origin of frame $\{M_0\}$ can be located at the center of mass of the system and the directions of the axes are then oriented along the principal inertial directions. The configuration of the overall formation can again be written in terms of the configuration of the team-frame (determined by 3 parameters) and $2n$ parameters defining the relative locations of the individual robots and can be calculated in the same way as was done for the above case given by Equation 3.35. Assigning the team-fixed frame in such a manner has the advantage that despite the added initial computation burden, such a selection makes the kinetic energy metric diagonal and allows ease of subsequent repeated evaluations of the system kinetic energy.

Motion Parameterization

Given a curve $A(s):[0, s_0] \rightarrow SE(2)$ and assuming a time parameterization, $s(t):[t_1, t_2] \rightarrow [0, s_0]$, the configuration of the body can be represented by:

$$A(s(t)) = \begin{bmatrix} R(s(t)) & \bar{p}(s(t)) \\ 0 & 1 \end{bmatrix} \in SE(2) \quad 3.39$$

A curve on $SE(2)$ physically represents a motion of the rigid body. In the rest of this thesis, we assume a constant speed of travel along the curve with $\dot{s} = 1$. An element $T(s(t))$ of the Lie algebra $se(2)$ can be associated to the tangent vector $\dot{A}(s(t))$ along the curve at $s(t)$ by a left translation as:

$$T(s(t)) = [A(s(t))]^{-1} \dot{A}(s(t)) = \begin{bmatrix} [\hat{\omega}] & R^T \dot{\bar{p}} \\ 0 & 0 \end{bmatrix} \quad 3.40$$

where $[\hat{\omega}] = R^T \dot{R}$ is the skew symmetric matrix corresponding to the vector $\bar{\omega}$. The choice of associating the element of the Lie Algebra with an element from the tangent space by left translation results in a body-fixed representation of twists that is invariant with respect to location of the inertial frame (and hence the preferred description for locomotion systems). If $t(s) = [\bar{\omega}^T \quad \bar{v}^T]^T$ is the vector pair representation of the matrix twist $T(s)$, then $\bar{\omega}$ corresponds to the angular velocity of the virtual structure while \bar{v} is the linear velocity of the origin O of $\{M_0\}$, both expressed in the team frame $\{M_0\}$.

An instantaneous screw axis can be associated with each twist. In general motion along an arbitrary path, instantaneous screw axis changes with time. However, for a certain class of motions, the twist and thus corresponding screw axis remains fixed. Such

motions are known as screw motions. For a planar case, the screw axis reduces to “pole” and such motion can be considered as rotations about a fixed pole with a constant angular velocity.

Chapter 4

Motion Planning

The main focus of this chapter is to develop a Geometric Motion Planning Strategy (GMPS) that considers the nonholonomic constraints of the Mobile Manipulators (MMs). Euler's theorem states that any displacement of a rigid body in a plane can be described by a pure rotation about a fixed point. Applying this theorem instantaneously, for any given path, it is possible to find a point such that motion is a pure rotation about this point at that instant of time. This point is called Instantaneous Center of Rotation (ICR) or pole of the motion. However, we do note that for arbitrary curves, the location of ICR keeps on changing and we include this within our GMPS framework.

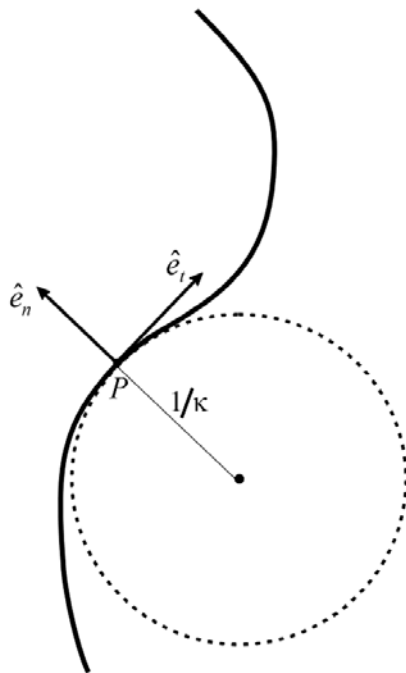


FIGURE 4-1: SERRET-FRENNET FRAME AND CURVATURE

Serret-Frenet Frame

Given an arc-length parameterized planar path $X : [0, s_0] \rightarrow \mathbb{R}^2$; $\vec{X}(s) = (x(s), y(s))$, a unit tangent vector \hat{e}_t can be computed for any point on curve, by taking derivative of the curve with respect to the parameter s . A unit normal vector can then be computed such that it is orthogonal to the unit vector.

$$\hat{e}_t(s) \cdot \hat{e}_n(s) = 0 \quad 4.1$$

where \cdot is the natural inner product defined on \mathbb{R}^2 . Additionally we require that \hat{e}_t and \hat{e}_n form a right handed coordinate frame. This frame is known as the Serret-Frenet frame and the evolution equations of this frame as one traverses along the length of the curve, may be expressed as:

$$\begin{bmatrix} \hat{e}_t'(s) \\ \hat{e}_n'(s) \end{bmatrix} = \begin{bmatrix} 0 & \kappa(s) \\ -\kappa(s) & 0 \end{bmatrix} \begin{bmatrix} \hat{e}_t(s) \\ \hat{e}_n(s) \end{bmatrix} \quad 4.2$$

where ' denotes differentiation with respect to the parameter s and $\kappa(s)$ is called curvature of the curve.

Curvature Of A Curve

The curvature of a curve is a measure of the rate of deviation of a curve from its instantaneous tangential direction as one proceeds along the length of the curve. Formally, the curvature $\kappa(s)$ is defined as the rate of change of angle φ made by the unit tangent vector with respect to the X axis of a suitable inertial frame OXY as one traverses along the length of the parametric plane curve defined by $x = x(s)$ and $y = y(s)$.

$$\kappa(s) = \frac{d\varphi}{ds} \quad 4.3$$

From the definition of slope of a curve,

$$\tan \varphi = \frac{dy}{dx} = \frac{dy/ds}{dx/ds} = \frac{y'}{x'} \quad 4.4$$

Differentiating Equation 4.4 with respect to arc-length gives

$$\frac{d(\tan \varphi)}{ds} = \sec^2 \varphi \frac{d\varphi}{ds} = \frac{x' y'' - x'' y'}{x'^2} \quad 4.5$$

Equation 4.5 allows us to express the curvature $\kappa(s)$ with respect to the first and second path derivatives as:

$$\kappa = \frac{d\varphi}{ds} = \left(\frac{x' y'' - x'' y'}{x'^2} \right) \frac{1}{\sec^2 \varphi} = \frac{x' y'' - x'' y'}{(x'^2 + y'^2)^{3/2}} \quad 4.6$$

The curvature is also related to the radius of curvature of an osculating circle (circle that shares the same tangent as that of the curve at a given point). Consider a tangent circle at a point on curve specified parametrically by

$$\begin{aligned} x &= r \cos u \\ y &= r \sin u \end{aligned} \quad 4.7$$

The curvature for this circle is then given by

$$\kappa = \frac{x' y'' - x'' y'}{(x'^2 + y'^2)^{3/2}} = \frac{r^2}{r^3} = \frac{1}{r} \quad 4.8$$

Thus, the radius of curvature r , of an osculating circle at a point on the curve is equal to $1/\kappa$. If the Serret-Frenet frame is considered to be the mobbing frame then the center of this circle corresponds to the location of ICR.

Note that in order to find the Serret-Frenet Frame and curvature, it was assumed that an arc-length parameterized curve is given. However, as discussed in Chapter 2, an arc-length parameterized curve can be generated from any extrinsic or intrinsic curve or even for a given set of data points. Hence, the above derivation is valid for any general planar path.

Rigid (and Non-rigid) Virtual Structure

Consider a virtual structure formed by n differentially driven nonholonomic MMs together with a team-fixed formation frame $\{M_0\}$ created by one of the ways as discussed in Chapter 3. We now require this team frame $\{M_0\}$ to be aligned with the Frenet-Serret frame at all the times. Thus the motion of the Serret-Frenet frame along the given path induces a parametric motion on the vertices of the virtual structure creating a velocity vector field. In particular, when one considers the case of rigid virtual structure formed using Type III modules, the velocity field, thus induced, because of the motion of the rigid virtual structure is called *helical velocity vector field*.

For a given time parameterization of the travel along the curve $s(t):[t_1, t_2] \rightarrow [0, s_0]$ let \dot{s} be the magnitude of velocity at which the frame travels along the path. The forward velocity of the origin of the Serret-Frenet, and thus, team-fixed

frame, ${}^{M_0}\mathbf{v}$ and its angular velocity ${}^{M_0}\boldsymbol{\omega}$ (as expressed in the moving Serret-Frenet frame) may be written as:

$$\begin{aligned} {}^{M_0}\mathbf{v} &= \hat{\mathbf{e}}_t \dot{s} \\ {}^{M_0}\boldsymbol{\omega} &= \dot{\hat{\mathbf{e}}}_t = \hat{\mathbf{e}}_k \kappa \dot{s} \end{aligned} \tag{4.9}$$

Geometric Motion Planning Strategy

Maintaining formation now means creating a rigid virtual structure and therefore, creates a requirement for a helicoidal velocity field at every vertex. In this work, we assume that frame $\{M_0\}$ travels along the path with constant $\dot{s}=1$ leaving the case of path- and time-varying $\dot{s}(s,t)$ for future work. As is often the case with locomotion systems, the description of the motion planning strategy and the formations becomes very simple when expressed in frame $\{M_0\}$. For the following discussion, unless otherwise specified, the frame of reference is team-fixed frame $\{M_0\}$. The motion of the team frame $\{M_0\}$ as it traces the desired path induces a helicoidal velocity field at the vertices of the virtual structure. The velocity of the i^{th} robot with respect to frame $\{M_0\}$ is computed as:

$${}^{M_0} \begin{bmatrix} \vec{v}_i \\ 0 \end{bmatrix} = {}^{M_0} \begin{bmatrix} {}^F T_{M_0} \end{bmatrix} \begin{bmatrix} \vec{r}_i \\ 1 \end{bmatrix} = \begin{bmatrix} 0 & -\kappa(s) & 1 \\ \kappa(s) & 0 & 0 \\ 0 & 0 & 0 \end{bmatrix} \begin{bmatrix} r_i \cos \theta_i \\ r_i \sin \theta_i \\ 1 \end{bmatrix} \tag{4.10}$$

As the formation maneuvers maintaining the rigidity of this virtual structure, our GMPS aligns the direction of forward travel (the X axis of each robot) with the induced velocity vector field.

This GMPS for developing motion plans for the individual mobile robots can be visualized using the notion of the ICR. In frame $\{M\}$, the location of ICR of the osculating circle is given by $(0, -1/\kappa(s))$. Graphically we see that the ICR of each individual WMR is constrained to lie on the line passing through the axle of each robot (Figure 4-2). Thus, when multiple robots form part of a virtual structure moving with its velocity vector field, the ICR of each robot must now coincide with the ICR of the virtual structure (and thus the motions along the underlying path). This factor then uniquely determines the orientation of each robot given its relative position with respect to the formation frame. As noted in Chapter 3, the configuration vector did not include orientation of each individual robot within the formation, since it is dependent variable and can be uniquely determined as an outcome of the overall GMPS.

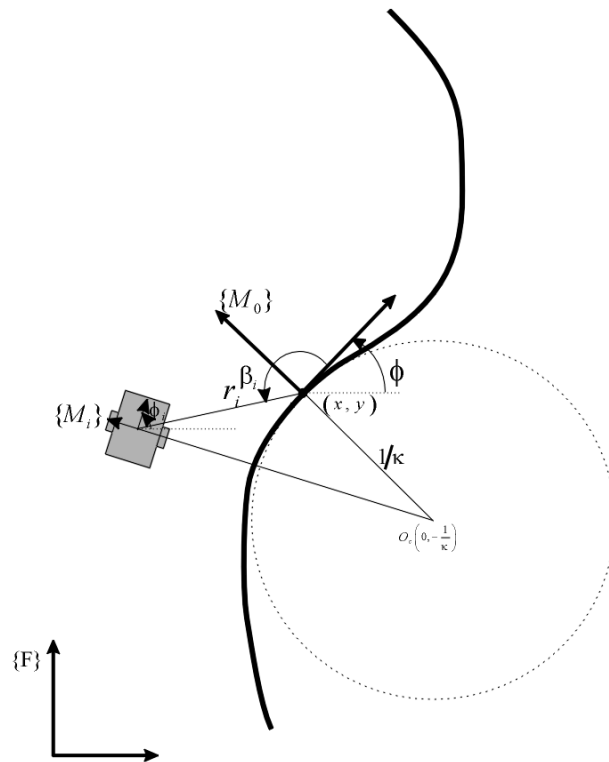


FIGURE 4-2: VISUALIZATION OF INSTANTANEOUS CENTER OF ROTATION CONSTRAINT

The corresponding twist vectors of the frames $\{M_i\}$, as they move to align themselves with this motion plan have a simplified representation in robot fixed frame $\{M_i\}$ as:

$${}^{M_i} \begin{bmatrix} F \\ t_{M_i} \end{bmatrix} = \begin{bmatrix} 1 \\ 0 \\ 0 \end{bmatrix} \omega_i + \begin{bmatrix} 0 \\ 1 \\ 0 \end{bmatrix} v_i \quad 4.11$$

where $v_i = \|\vec{v}_i\|$ and ω_i are the magnitudes of the linear and angular velocities of the i^{th} robot.

However, for any given path, the relative configurations (\vec{r}_i) induce different motion plans (with different performance characteristics) for the individual mobile robots as they move in formation towards the final goal. Hence, using the performance metrics discussed in Chapter 2, we can evaluate the performance at each of these different configurations and use this to optimize the relative location.

Note that in the above discussion, it was assumed that a prescribed *path* was given and then the twist of the frame $\{M_0\}$, was calculated using the parametric equation of the curve. However, an online implementation of the GMPS is also possible given only the instantaneous motion representation (twist) of a suitable task-fixed frame. Consider a frame $\{M_0\}$ moving with linear velocity ${}^M \vec{v}$ and angular velocity ${}^M \vec{\omega}$. If this velocity ${}^M \vec{v}$ and ${}^M \vec{\omega}$ corresponds to unit velocity along an underlying curve, then from Equation 4.9, it is clear that $\kappa = {}^M \vec{\omega}$. The location of ICR is thus given by $(0, -1/\omega)$. Using this

information, the helicoidal velocity vector field can be generated and the frames $\{M_i\}$ on the manipulators can now be oriented in the direction of this vector field at their location.

Chapter 5

Formation Motion Planning

In this chapter, a case study of three mobile robots, moving in a formation, is considered and we present the results of the application of the Geometric Motion Planning Strategy (GMPS) developed in previous chapter to this formation. We first obtain and discuss the results of our GMPS for some special paths (for which analytical results are possible). Subsequently, we consider a general case and present results for this case.

Problem Formulation

Consider a system of three nonholonomic Wheeled Mobile Robots (WMRs) maneuvering in a plane. Note that the procedure is scalable and can be generalized for n mobile robots case. Let the distance of each mobile robot from the team-fixed frame $\{M_0\}$ be r_i and the angle be represented by β_i as shown in Figure 5-1 where $i=1,2,3$. The configuration vector for the overall formation is

$$q = (g_0, \vec{r}, \vec{\beta}) \in Q = SE(2) \times \mathbb{R}^n \times T^n \quad 5.1$$

We require this formation to follow an arc-length parameterized planar path

$$X : [0, s_0] \rightarrow \mathbb{R}^2; \quad \vec{X}(s) = (x(s), y(s)) \quad 5.2$$

Since the WMRs are not constrained with respect to each other, the formation can follow the planar path with infinitely many configurations. However, these different configurations influence the performance of the system.

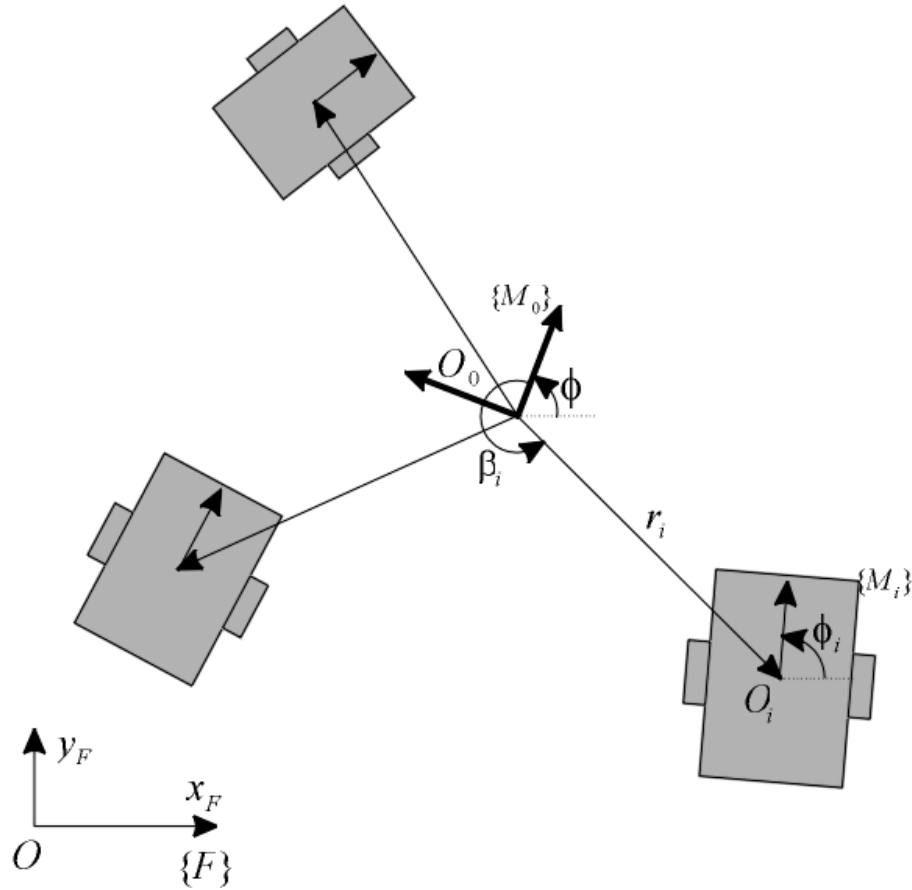


FIGURE 5-1: UNCONSTRAINED FORMATION OF WHEELED MOBILE ROBOTS

Thus, the aim is to find the “best” possible configuration of the formation of WMRs which will move along a desired path. To aid this process, we develop performance measures using Klein Metric and the decoupled Park (Kinetic Energy) metric (Zefran, 1996). The maximum/minimum of these quantitative performance measures is used to find the “best” configuration.

Intuitively the optimal solution arrived at by using these metrics could be such that that all WMRs will gather in a small space. Hence, additional “regional” constraints of the sort explained in Figure 5-2 are imposed on the problem in order to limit the locations of individual WMRs to specific sectors relative to the frame $\{M_0\}$.

As seen in the Figure 5-2, the shape space of the formation is restricted such that each WMR lies within two circles of radii r_{\min} and r_{\max} centered at origin of $\{M_0\}$ and within selected orientational ranges with respect to the frame $\{M_0\}$.

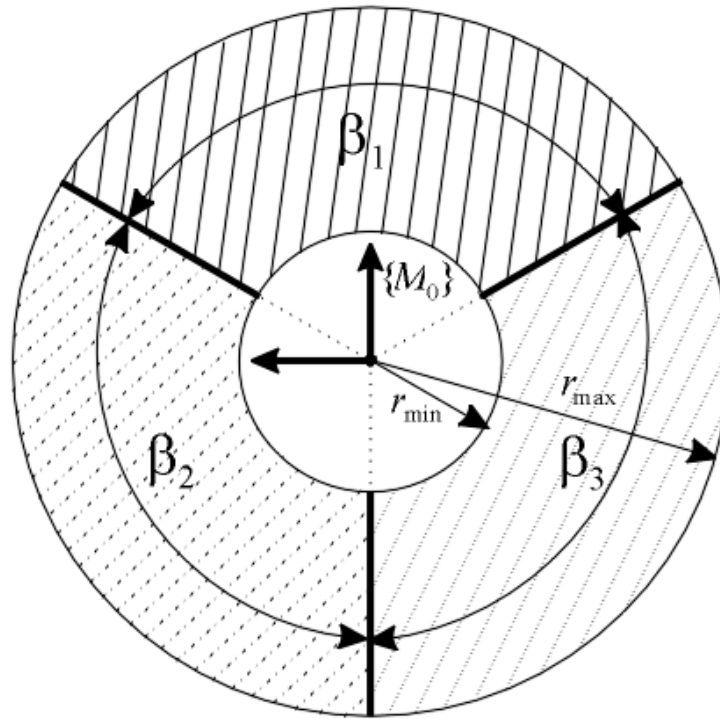


FIGURE 5-2: CREATION OF SECTORS FOR FEASIBLE LOCATIONS OF INDIVIDUAL ROBOTS

Constraining the problem in this way reduces the feasible solution space but is useful to allow some user control over the relative locations of the WMRs within the formation. Most often the choice of parameters r_{\min} , r_{\max} , β_1 , β_2 and β_3 is entirely at the designers' discretion. However, we note that in some cases the physical structure of the problem may impose limits as is discussed during the formation payload transport application in Chapter 6.

Screw Motion

A screw motion is the one in which the twist remains constant throughout the motion. Constant twist motions where $v = const$ and $\omega = const$ results in circular (and in limit straight line) trajectories for frame $\{M_0\}$. Further, the angular velocity of each robot ω_i becomes identical to the angular velocity ω of frame $\{M\}$.

Virtual Experiment

We perform a virtual experiment for evaluating the performance of a formation of WMRs as it follows a screw motion in following steps:

1. Selecting the path for $\{M_0\}$ to be a circle of unit radius, 12 equally spaced points from this path are chosen to serve as the given path specification. Note that, however, it is not necessary to take uniformly distributed initial dataset.
2. Using the Euclidean distances between points as the initial parameterization, we develop a cubic spline interpolation of the given data points and subsequently, iteratively refined this parameterization to obtain an arc-length parameterization as discussed in Chapter 2.
3. Using a Serret-Frenet frame moving along the length of the arc-length parameterized curve with a velocity $\dot{s}=1$, the linear velocity $v = [x'(s) \ y'(s)]^T$ and acceleration $a = [x''(s) \ y''(s)]^T$ of this

Serret-Frenet frame can be calculated with the help of the approximated cubic spline equations as discussed in Chapter 2.

4. Using the theory explained in Chapter 2, the curvature of the path

$$\kappa = \frac{x'y'' - y'x''}{(x'^2 + y'^2)^{3/2}}$$

can be calculated. The angular velocity of the Serret-

Frenet frame can now be given as $\omega = \kappa \dot{s} = \kappa$ as $\dot{s} = 1$ and the radius of the osculating circle at any instant as $r_c = 1/\kappa$

5. Forcing the frame $\{M_0\}$ always to be coincident with this Serret-Frenet frame as per our GMPS, the velocities of the individual WMRs can be determined to be ${}^{M_0}\vec{v}_i = {}^{M_0}\vec{v}_0 + \hat{\omega}_0 \vec{r}_i$ where ${}^{M_0}\vec{v}_0 = [1 \ 0 \ 0]^T$ and

$$\hat{\omega}_0 = \begin{bmatrix} 0 & -\kappa \\ \kappa & 0 \end{bmatrix}.$$

6. It is important to emphasize here that for a general case, the angular velocity ω_i of individual WMRs is different from the angular velocity ω_0 of team-fixed frame $\{M_0\}$. The angular velocity ω_i of individual mobile robots can be determined from the velocity ${}^{M_0}\vec{v}_i$ as $\omega_i = \|\|{}^{M_0}\vec{v}_i\| / O_i O_c$ where $O_i O_c$ is the distance between the origin of frame $\{M_i\}$ and the center of the instantaneous circle O_c

7. Calculate the Klein Metric $(\alpha\omega_i^2)$ and Kinetic Energy Metric

$$\frac{1}{2}(I_{zz}\omega^2 + mv^2).$$

Klein Metric Results

Since, ω_i is constant, the Klien metric ($\alpha\omega_i^2$) results in a constant value for the performance measure for all possible relative configurations. The numerical results obtained from the virtual experiment by varying r_i and β_i while the robot is undergoing a screw motion also yields a near constant value of the Klein performance metric.

Kinetic Energy Metric Results

An analytical solution for the optimal angular configuration for a screw motion using Park Decoupled Kinetic Energy metric can be found from the geometry of the problem.

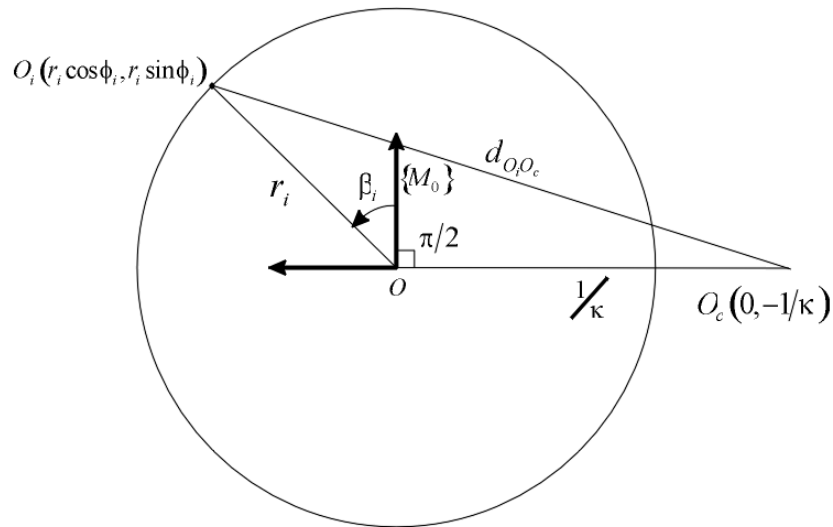


FIGURE 5-3: ANALYTICAL SOLUTION FOR OPTIMAL CONFIGURATION

Consider a team fixed frame $\{M_0\}$ and origin O_i of mobile robot frame $\{M_i\}$ at distance r_i and angle β_i as shown in Figure 5-3. The curvature κ of the curve at a point is inverse of the radius of curvature of the path at that point. Hence, the location of the Instantaneous Center of Rotation (ICR) O_c is $(0, -1/\kappa)$. Using the cosine rule gives

$$d_{o,o_c}^2 = r_i^2 + \frac{1}{\kappa^2} - 2r \cos\left(\frac{\pi}{2} + \beta_i\right) \quad 5.3$$

The scalar expression for the Kinetic Energy using the Decoupled Kinetic Energy Metric can be written as:

$$\mathbf{E} = \begin{bmatrix} \vec{\omega}_i \\ \vec{v}_i \end{bmatrix}^T \begin{bmatrix} I_{zz} & 0_{1 \times 2} \\ 0_{2 \times 1} & mI_{2 \times 2} \end{bmatrix} \begin{bmatrix} \vec{\omega}_i \\ \vec{v}_i \end{bmatrix} = \vec{\omega}_i^2 + m\vec{v}_i^2 \quad 5.4$$

Given ω of frame $\{M\}$ and the fact that the velocity of ICR is instantly zero, gives us the relation in Equation 5.5

$$v_i = \omega d_{o,o_c} \quad 5.5$$

Combining Equations 5.3 and 5.4 and substituting into Equation 5.5, we get:

$$\mathbf{E} = v_i^2 \left(\frac{\kappa^2}{1 + \kappa^2 r_i^2 - 2r_i \kappa \cos(\pi/2 + \beta_i)} + m \right) \quad 5.6$$

The minimum of this energy expression with respect to orientations can be found by differentiating Equation 5.6 with respect to β_i and equating it to zero. The value of β_i thus calculated is:

$$\beta^* = -\frac{\pi}{2} \quad 5.7$$

Similarly, the minimum energy with respect to r_i can be found by differentiating Equation 5.6 with respect to r_i and equating it to zero. The condition for which the expression gives minimum energy is given as:

$$r^* = \frac{\cos\left(\frac{\pi}{2} + \beta\right)}{\kappa}$$

5.8

The plots obtained from these results are shown in Figure 5-4. The results are plotted for $v = 2\pi, \omega = 1$. It can be seen that the optimal value of β_i^* is constant at $\pi/2$ for all values of r_i . This means that for “best” configuration, the WMR should always be located as close to IC as possible because the velocity of the mobile robot is directly proportional to its distance from the location of IC. If the robot is located at IC, the velocity is zero.

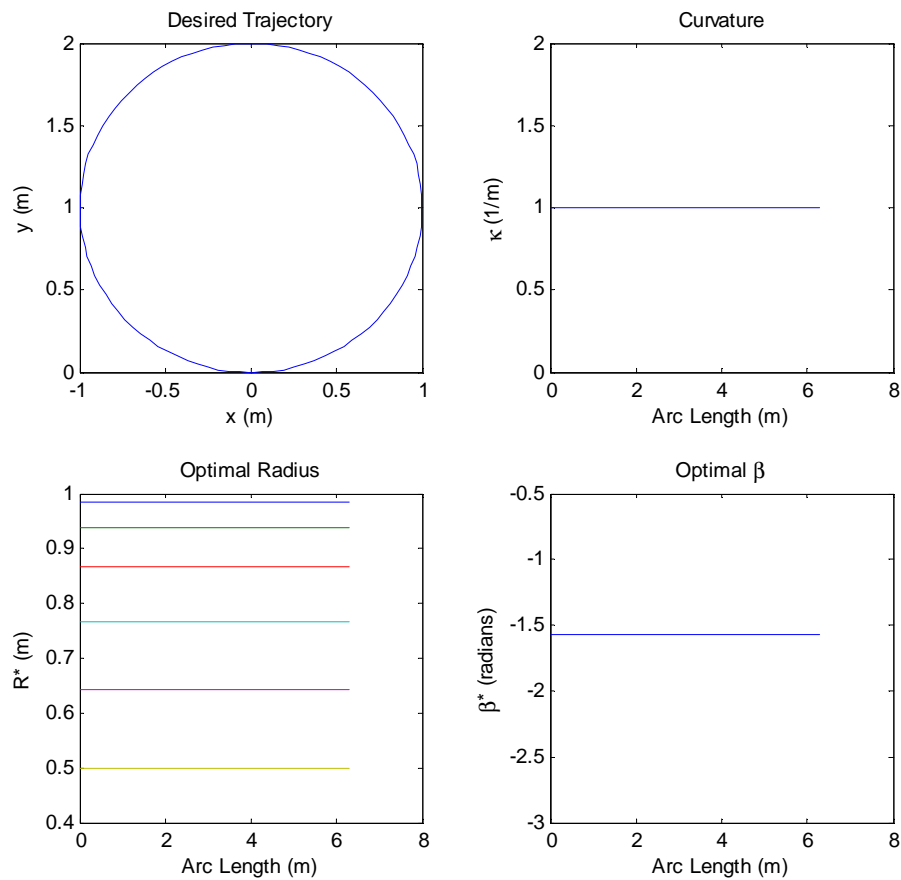


FIGURE 5-4: ANALYTICAL RESULTS FOR SCREW MOTION

The numerical implementation of the optimization algorithm yields similar results. Figure 5-5 shows the results for the screw motion case using the Kinetic Energy Metric.

O_i 's are the location of the optimal position. It can be seen that each O_i tries to be as near to ICR location as possible. However, due to side constraints on the feasible values of θ_i^i 's the above configuration is the best configuration.

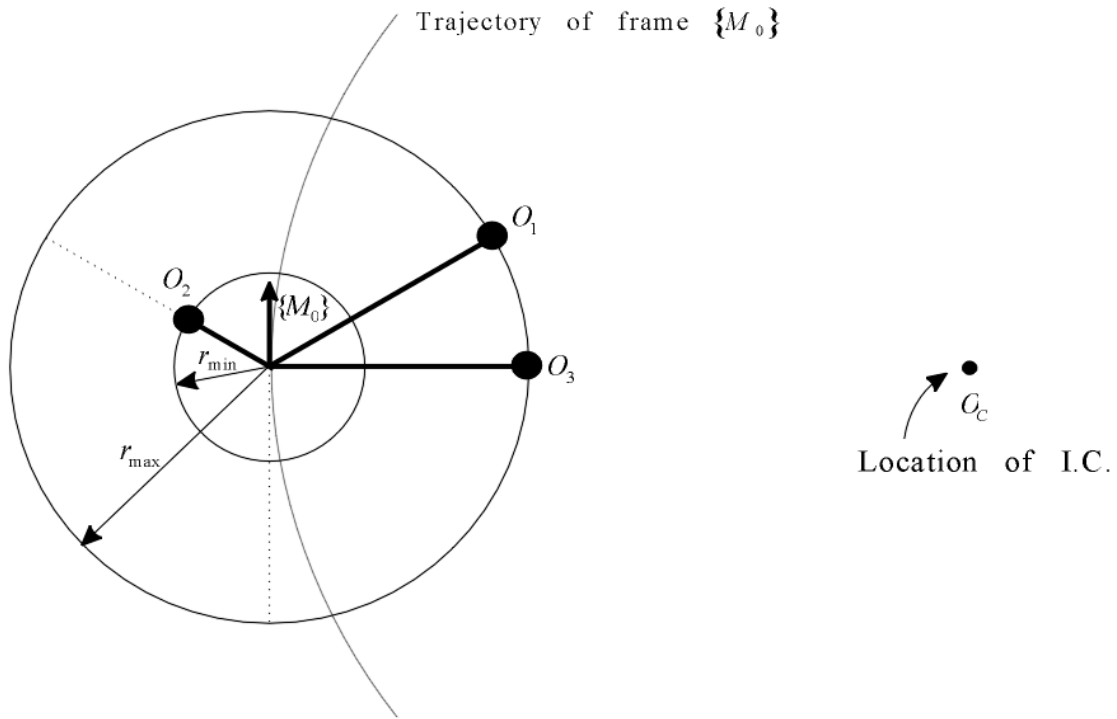


FIGURE 5-5: OPTIMAL CONFIGURATION FOR FOLLOWING A SCREW MOTION (OBTAINED NUMERICALLY)

Non-Screw (Sinusoidal) Motion

While a sinusoidal path does not correspond to a screw motion, one can still derive analytical expressions for this standard curve. In light of Equation 5.8, it can be seen that the value of optimal length r_i^* depends on the value of κ . In the case of

sinusoidal path, the curvature keeps on changing with time. However, analytical expression of κ can be derived. Consider a sinusoidal curve parametrically represented by:

$$\begin{aligned} x &= a \sin(\omega t) \\ y &= t \end{aligned} \quad 5.9$$

The arc-length of this curve is given by

$$s(t) = \int \sqrt{R'^2} dt \quad 5.10$$

where

$$R = a \sin(\omega t) \hat{i} + t \hat{j} \quad 5.11$$

R' is the derivative of R with respect to arc-length s and is given by:

$$R' = \frac{dR}{ds} = \frac{dR/dt}{ds/dt} = \frac{a\omega \cos(\omega t) \hat{i} + \hat{j}}{\sqrt{1 + a^2 \omega^2 \cos^2(\omega t)}} \quad 5.12$$

Taking second derivative of R with respect to arc-length s gives

$$R''(s) = \frac{-a\omega^2 \sin(\omega t) \hat{i}}{1 + a^2 \omega^2 \cos^2(\omega t)} \quad 5.13$$

Curvature of the curve κ given by $\kappa = \|R''(s)\|$ thus becomes

$$\kappa = \frac{a\omega^2 \sin(\omega t)}{1 + a^2 \omega^2 \cos^2(\omega t)} \quad 5.14$$

The analytical results are shown in Figure 5-6. The desired trajectory is a sinusoidal wave. The curvature, as shown in upper-right plot, diminishes to zero at certain points and thus the radius of curvature r_i^* thus should tend to infinity at those

points. However, in the numerical implementation/program, a limit on the maximum value of r_i^* is placed at $(-2, 2)$.

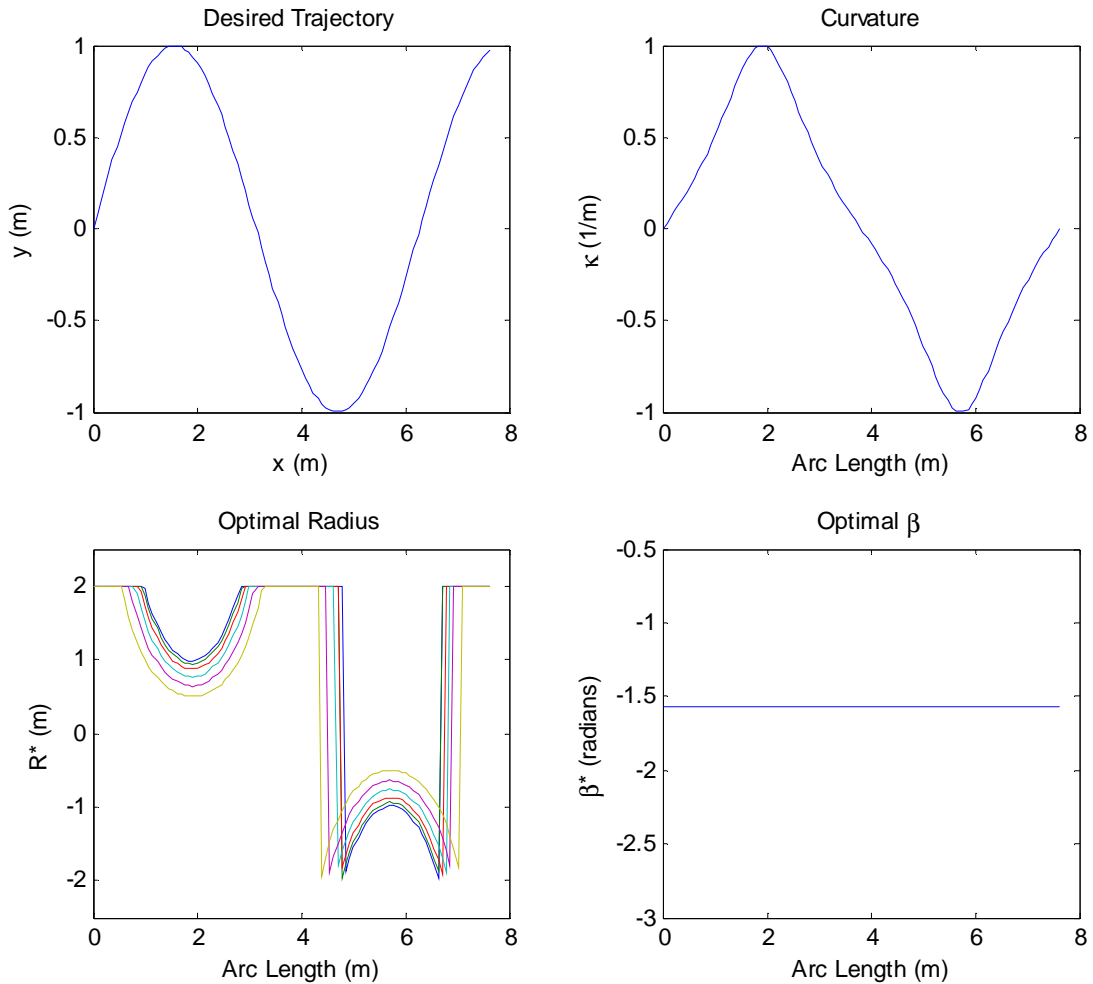


FIGURE 5-6: ANALYTICAL RESULTS FOR NON-SCREW (SINUSOIDAL) MOTION

Figure 5-7 shows the comparison of the value of κ obtained by analytical and numerical approach. The observed error can be attributed to the fact that in numerical analysis, a sine curve is approximated by a series of cubic spline connected at fixed points. Hence, for a better approximation, higher order splines, such as quintic splines, would be desirable.

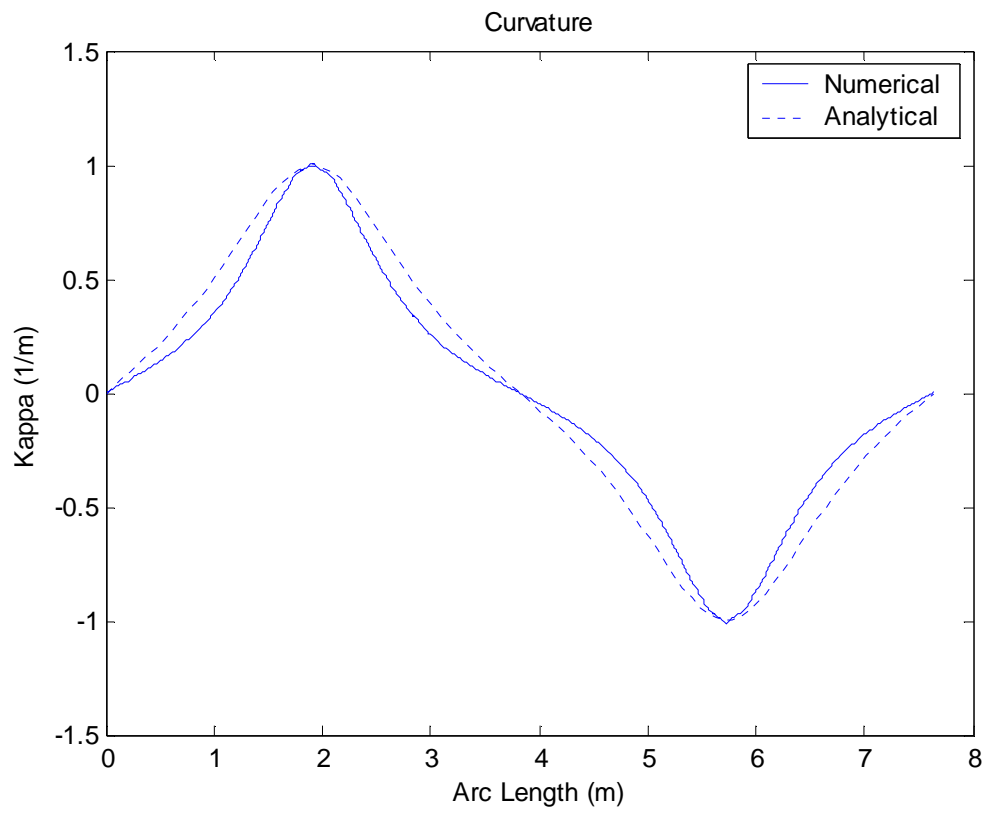


FIGURE 5-7: COMPARISON BETWEEN NUMERICAL AND ANALYTICAL VALUES OF κ

Chapter 6

Formation Payload Transport

In this chapter, the results developed in previous chapter are applied to a formation of Mobile Manipulator (MM) modules of Type I, Type II and Type III as they transport a payload. First we discuss the pros and cons of using the simplest module of Type III. Subsequently we motivate the necessity of more complex modules and then describe the use and implementation of results developed in Chapter 5 using the type I module by deriving equivalence between the centralized task frame based parameterization and individual MM module based parameterization.

Type III: R Mobile Manipulator Module

The Type III module is the simplest MM configuration that can be used for payload transport. However, it is also the most restrictive case. Hence, while implementation of formations using a Type III module is least complex, there are significant limits on its performance as we discuss in this section. As can be seen from Figure 6-1, when Type III MM is employed to transport a payload, the payload and the MMs form a **rigid virtual structure**. Thus, after the initial placement, we see that the relative locations of the modules cannot be altered and we cannot change the formation shape at intermediate times in order to reduce value of the performance measure.

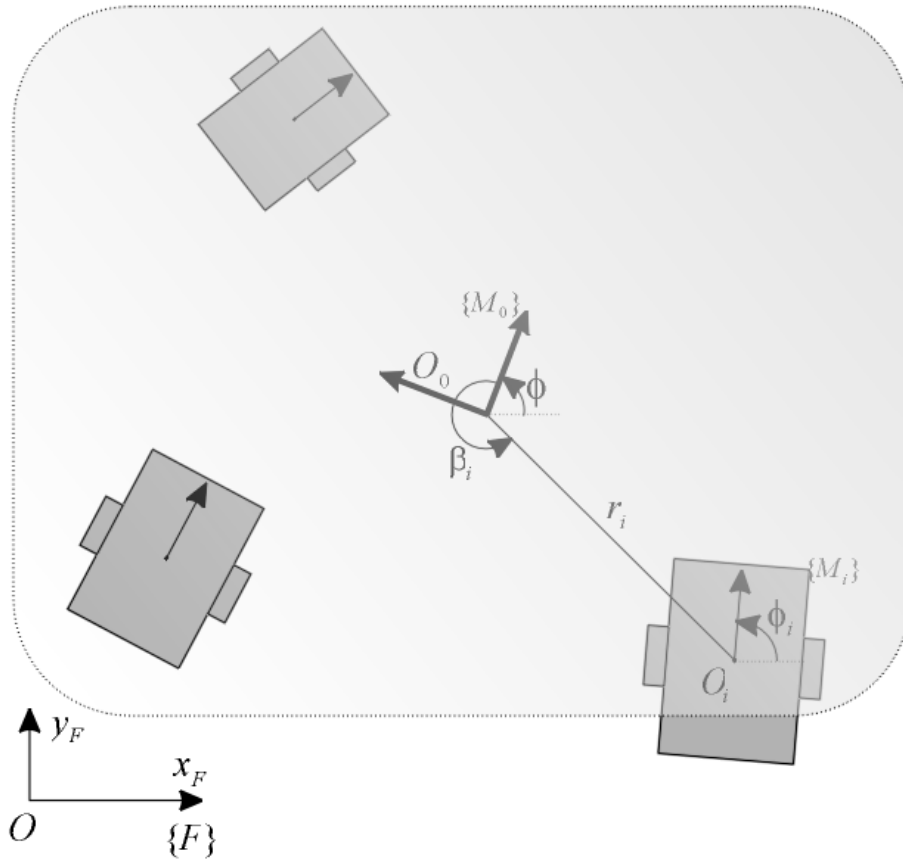


FIGURE 6-1: FORMATION OF TYPE III MODULES WITH A PAYLOAD

Screw Motion

For different kinds of screw motions (which includes circles with different radii and straight lines), the optimal configuration remains the same along the entire curve. Hence, a suitable arrangement of these Type III modules in the optimal configuration at the start position is adequate for it to remain optimal for the entire path.

Non-Screw (Sinusoidal) Motion

However, as can be seen from the analytical results, for a sinusoidal motion, or for any general motion, the optimal configuration keeps changing with the location of the frame $\{M\}$. Hence, the configuration optimized for a screw-motion, is usually not

optimal for the general motion. In such cases we integrate the metric along the length of curve for different configurations, and then find that configuration which minimizes the performance measure integrated along the path. This can be written as

$$TPM = \int_0^{s_0} PM(s, q) ds \quad 6.1$$

where TPM is the Total Performance Measure obtained by integrating the performance measure along the length of the curve and PM is the performance measure at each point along the length of curve. However, the performance obtained in this manner will in general not be as good as the case where we can dynamically change the configuration.

Type II: RR Mobile Manipulator Module

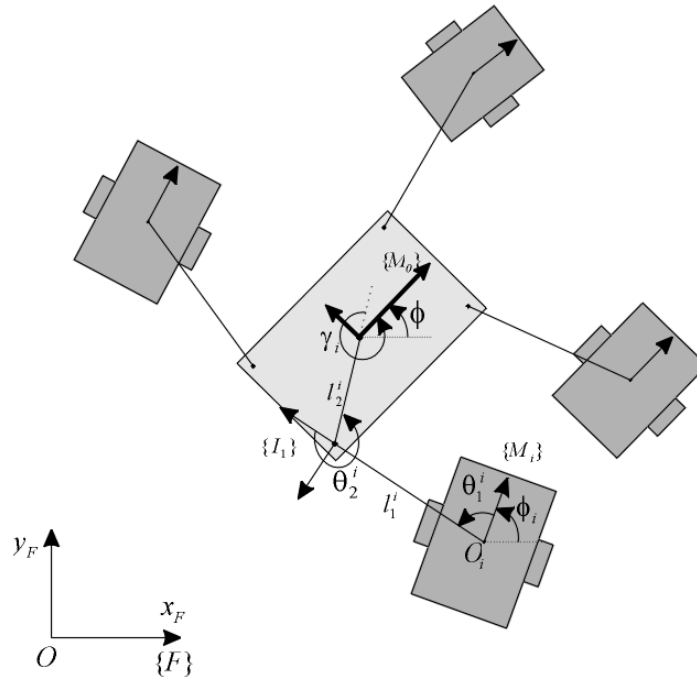


FIGURE 6-2: FORMATION OF TYPE II MODULES WITH A PAYLOAD

Type II modules offer some freedom in allowing the mobile bases to move with respect to the frame $\{M\}$. Note that we consider the second link of Type II modules

merged with the payload and thus the point of attachment to the payload is $\{I_1\}$. However, it is clear from Figure 6-2 that these modules are also restrictive in the sense that the location of the mobile bases $\{M_i\}$ are constrained to lie on a circle with respect to the point of attachment to the payload $\{I_1\}$. Hence, we avoid a discussion of this case and focus our attention to a detailed discussion of payload transport with the Type I modules directly.

Type I: RRR Mobile Manipulator Module

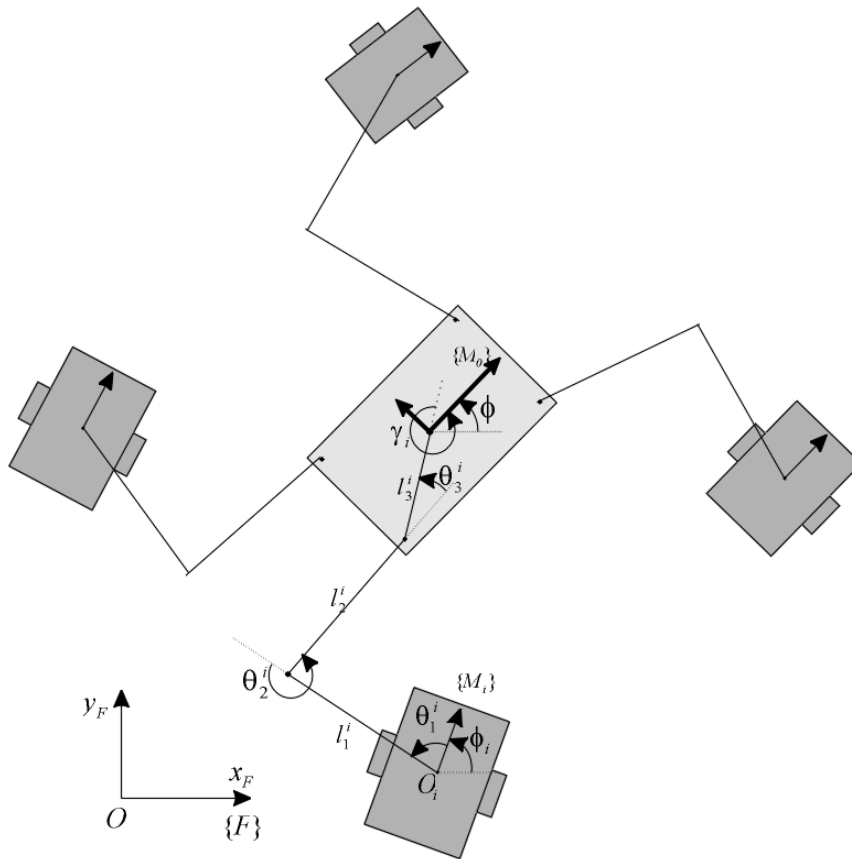


FIGURE 6-3: FORMATION OF TYPE I MODULES WITH A PAYLOAD (PARAMETERIZATION LOCAL TO EACH MOBILE MANIPULATOR)

This is the most general type of MM module used in this thesis. Figure 6-3 shows a system of four Type I modules carrying a common payload. Note that we treat the final

link of each type of Type I module as merged with the payload and hence, without loss of generality, the point of attachment is considered to be coincident with $\{I_2\}$.

The homogeneous transform ${}^F A_{M_0}$ is given as

$${}^F A_{M_0} = {}^F A_{M_i} {}^{M_i} A_{E_{1i}} {}^{E_{1i}} A_{E_{2i}} {}^{E_{2i}} A_{M_0} \quad 6.2$$

Expressing everything in frame $\{M_0\}$

$$\left[{}^F A_{M_i} \right]^{-1} {}^F A_{M_0} = {}^{M_i} A_{E_{1i}}(\theta_{1i}) {}^{E_{1i}} A_{E_{2i}}(\theta_{2i}) {}^{E_{2i}} A_{M_0}(\theta_{3i}) \quad 6.3$$

Simplifying the above equation yield,

$$\left[{}^F A_{M_i} \right]^{-1} {}^F A_{M_0} = \begin{bmatrix} \cos \Theta_i & -\sin \Theta_i & l_{1i} \cos \theta_{1i} + l_{2i} \cos(\theta_{1i} + \theta_{2i}) + l_{3i} \cos \Theta_i \\ \sin \Theta_i & \cos \Theta_i & l_{1i} \sin \theta_{1i} + l_{2i} \sin(\theta_{1i} + \theta_{2i}) + l_{3i} \sin \Theta_i \\ 0 & 0 & 1 \end{bmatrix} \quad 6.4$$

where $\Theta_i = (\theta_{1i} + \theta_{2i} + \theta_{3i})$

This parameterization of the formation is conducive to decentralized control where each robot governs itself relative to the moving frame.

Due to the redundancy introduced because of multi-link Manipulator mounted on the mobile base, we can place the MM anywhere within the feasible sector bounded by an inner circle with radius $|l_1 - l_2|$ and an outer circle with radius $|l_1 + l_2|$. Note that in this case the constraint r_{\min} corresponds to $|l_1 - l_2|$ and r_{\max} corresponds to $|l_1 + l_2|$. We can also now find a one-to-one correspondence between the parameterizations $q = (g_0, \vec{r}, \vec{\beta}) \in Q = SE(2) \times \mathbb{R}^n \times T^n$ and $g = ({}^F R_M, {}^F \vec{p}, \theta_1, \theta_2, \theta_3) \in SE(2) \times T^3$.

Equivalence of Parameterizations

In this section, we consider two variants of parameterizations of these Type III modules. The parameterization $q = (g_0, \vec{r}, \vec{\beta}) \in \mathcal{Q} = SE(2) \times \mathbb{R}^n \times T^n$ may be considered as an RPR linkage when we also consider the angle ϕ_i . From Figure 6-4, the homogeneous transform

$${}^F A_{M_i} = {}^F A_{M_0} {}^{M_0} A_{J_{1i}} {}^{J_{1i}} A_{J_{2i}} {}^{J_{2i}} A_{M_i} \quad 6.5$$

Expressing everything in frame $\{M_0\}$,

$$\left[{}^F A_{M_0} \right]^{-1} {}^F A_{M_i} = {}^{M_0} A_{J_{1i}} (\alpha_{1i}) {}^{J_{1i}} A_{J_{2i}} (r_i) {}^{J_{2i}} A_{M_i} (\alpha_{2i}) \quad 6.6$$

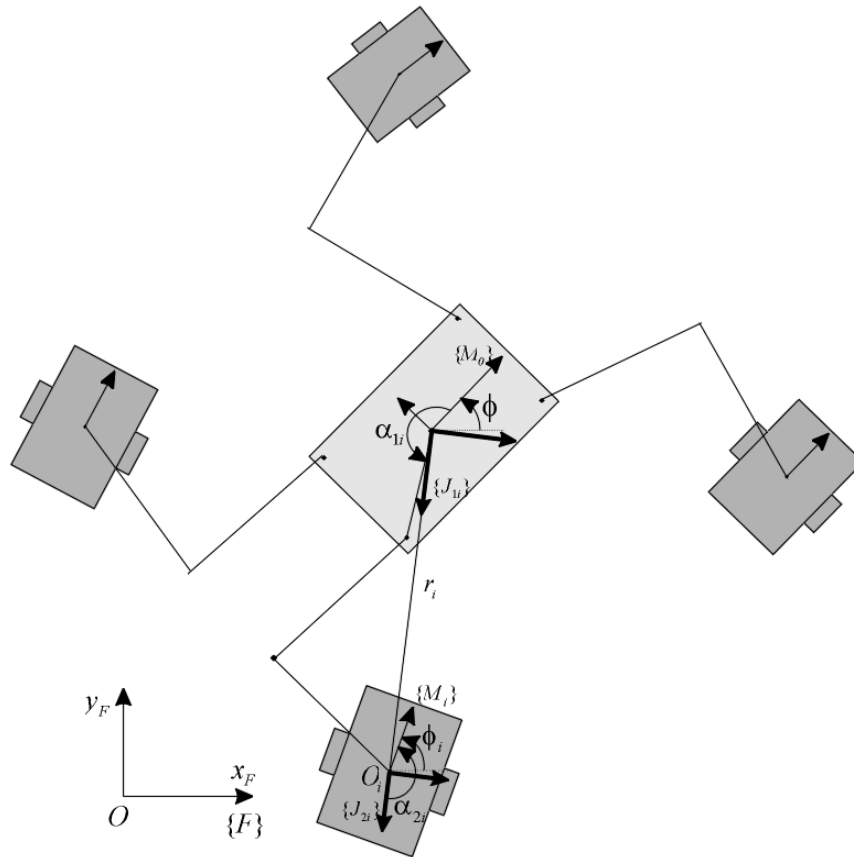


FIGURE 6-4: AN ALTERNATE PARAMETERIZATION OF FORMATION OF TYPE I MODULES (TASK FRAME BASED PARAMETERIZATION)

Simplifying the above equation,

$$\left[{}^F A_{M_0} \right]^{-1} {}^F A_{M_i} = \begin{bmatrix} \cos(\alpha_{1i} + \alpha_{2i}) & -\sin(\alpha_{1i} + \alpha_{2i}) & r_i \cos \alpha_{1i} \\ \sin(\alpha_{1i} + \alpha_{2i}) & \cos(\alpha_{1i} + \alpha_{2i}) & r_i \sin \alpha_{1i} \\ 0 & 0 & 1 \end{bmatrix} \quad 6.7$$

This is more conducive to treatment as a unified composite system where we have the description of the motion of the team frame relative to the inertial frame and a set of shape variables describing the relative position of the various robots relative to this common frame.

An alternate parameterization is also possible by considering the variables local to each MM as discussed in section on Type III MMs.

Multiplying the right hand sides of Equations 6.4 and 6.7,

$$\left[{}^F A_{M_0} \right]^{-1} {}^F A_{M_i} \left[{}^F A_{M_i} \right]^{-1} {}^F A_{M_0} = \left[{}^F A_{M_0} \right]^{-1} I {}^F A_{M_0} = I \quad 6.8$$

Performing the above matrix multiplication and simplifying,

$$\begin{bmatrix} \cos(\Gamma) & -\sin(\Gamma) & K_1 \\ \sin(\Gamma) & \cos(\Gamma) & K_2 \\ 0 & 0 & 1 \end{bmatrix} = I \quad 6.9$$

where

$$\begin{aligned} \Gamma &= \Theta_i + \alpha_{1i} + \alpha_{2i} \\ K_1 &= l_3 \cos \Gamma + l_2 \cos(\Gamma - \theta_{3i}) + l_1 \cos(\alpha_{1i} + \alpha_{2i} + \theta_{1i}) + r_i \cos \alpha_{1i} \\ K_2 &= l_3 \sin \Gamma + l_2 \sin(\Gamma - \theta_{3i}) + l_1 \sin(\alpha_{1i} + \alpha_{2i} + \theta_{1i}) + r_i \sin \alpha_{1i} \end{aligned} \quad 6.10$$

Hence, we can obtain one-to-one relationship between $(\theta_i, \theta_{2i}, \theta_{3i})$ and $(r_i, \alpha_i, \alpha_{2i})$ using Equation 6.8. Hence, all the results obtained before can be readily applied to the case of Type III modules.

In conclusion, Type I module allows larger feasible design space by allowing freedom to change the value of r_i along with α_i . This $2-\infty$ design space allows the system to accommodate external disturbances. By placing joint sensors at actuated and unactuated joints, the system can sense the changes in the configuration and the control algorithm can take corrective action based on these changes. Moreover, by adding redundant actuation by locating the actuators at the unactuated joints, the singular configurations can also be avoided.

Chapter 7

Conclusions and Future Work

Summary and Conclusion

In Chapter 1, we note that a modular, reconfigurable system is required to achieve the desired goal. Hence, in Chapter 3, we developed the twist based mathematical model for the most general case of a Mobile Manipulator (MM) after a brief mathematical background prepared in Chapter 2. Then, we specialized this MM in to Type I, Type II and Type III modules based on the simplifications.

In Chapter 4, we describe our Geometric Motion Planning Strategy (GMPS) which uses a geometric approach and directly takes into consideration the nonholonomic constraints that arises due to the Wheeled Mobile Manipulator (WMM) rather than considering them as point objects.

In Chapter 5, we determine the trajectories of individual MMs maneuvering in a formation, as the desired point (which in this case is team-fixed frame) traces the desired trajectory. We determine the results using analytical method for standard paths like circle and a sinusoidal wave and then compare these results with the ones obtained using the numerical method (program). This validates our hypothesis that by approximating a path as a series of cubic splines and determining the trajectories of individual modules gives similar results as if taking the exact continuous path.

Finally, in Chapter 6, we show how the results developed in Chapter 5 can be directly applied to the case when the modules are employed to transport a payload along a desired trajectory. We show equivalence between the centralized task frame based parameterization and individual MM module based parameterization.

In conclusion, we develop a method of motion planning that takes into consideration the nonholonomic constraints in the planning phase and optimizes the performance of the formation of robots using metrics defined on $SE(2)$. For the cases when analytical expressions were possible, we compare our numerical results with the analytical results. Finally, we showed how the results obtained using the GMPS can be applied to Type I, Type II and Type III modules as they cooperate to transport a payload.

Future Work

In this thesis, we concentrate on optimizing the performance of the formation using the energy metric. However, many different metrics are possible. With much of the ground work done in Chapter 3, the first step of future work may be to perform the optimization using manipulability metric. With the help of the Jacobian matrix and the equivalence between different parameterizations as shown in Chapter 6, it is easy to optimize the formation for a given path for maximum manipulability. The objective function in such case could be maximizing the inner product between the direction of major axis and the tangent direction to the path. The maximum value of the objective function being unity and the minimum value being nullity, the objective function is very well behaved.

Our work considers the velocity of Serret-Frenet frame along the given path to be $\dot{s} = 1$. Hence, another avenue in which one can take this work further is by determining optimal configuration for any given $\dot{s} = const$ or even more general case of \dot{s} being time varying.

Current work considers a cubic spline approximation of a given curve. Another area in which one can take this work further is by considering higher order polynomial approximation like a quintic polynomial in order to increase the accuracy of the results.

Bibliography

- [1] Arkin, R. C. and Bekey, G. A., 1997, (Eds.), *Robot Colonies*, Special Issue of Autonomous Robots, vol. 4 no. 5, reprinted by Kluwer Academic Publishers, Boston.
- [2] Angeles, J., 2002, *Fundamentals of Robotic Mechanical Systems: Theory, Methods and Algorithms*, Springer-Verlag New York, Inc., New York, NY, U.S.A
- [3] Beard, R. W., Lawton, J. and Hadaegh, F. Y., 2001, "A Feedback Architecture for Formation Control," *IEEE Transactions on Control Systems Technology*, vol. 9, no. 6, pp. 777-790.
- [4] Belta, C. and Kumar, V., 2002, "Trajectory Design for Formations of Robots by Kinetic Energy Shaping," in *Proceedings of IEEE International Conference on Robotics and Automation*, pp. 2593-2598, Washington, DC.
- [5] Bicchi, A. and Prattichizza, D., 2000, "Manipulability of Cooperating Robots with Unactuated Joints and Closed-Chain Mechanisms", *IEEE Transactions on Robotics and Automation*, vol. 16, no. 4, pp. 336 -345.
- [6] Balch, T. and Arkin, R. C., 1998, "Behavior-based Formation Control for Multiagent Robot Teams," *IEEE Transactions on Robotics and Automation*, vol. 14, no. 6, pp. 926-939.
- [7] Cao, Y., Fukunaga, A. S. and Kahng, A. B., 1997, "Cooperative Mobile Robotics: Antecedents and Directions," *Autonomous Robots*, vol. 4, no. 1, pp. 7-27.
- [8] Coxeter, H., 1969, *Introduction to Geometry*, John Wiley & Sons, Inc., New York, NY, U.S.A.
- [9] Desai, J. P., Ostrowski, J. P. and Kumar, V., 2001, "Modeling and Control of Formations of Nonholonomic Mobile Robots," *IEEE Transactions on Robotics and Automation*, vol. 17, no. 6, pp. 905-908.
- [10] Denavit, J. and Hartenberg, R. S., 1955, "A Kinematic Notation for Lower Pair Mechanisms," *Applied Mechanics*, Vol. 22, pp. 215-221.
- [11] Egerstedt, M. and Hu, X., 2001, "Formation Constrained Multi-agent Control," *IEEE Transactions on Robotics and Automation*, vol. 17, no. 6, pp. 947-951.
- [12] Gosselin, C. and Angeles, J., 1991, "A Global Performance Index for the Kinematic Optimization of Robotic Manipulators," *Journal of Mechanical Design*, vol.113. pp.220-226.
- [13] Wolfram - <http://mathworld.wolfram.com>

- [14] Lawton, J., Young, B. and Beard, R., 2000, "A Decentralized Approach to Elementary Formation Maneuvers," in *Proceedings of 2000 IEEE International Conference on Robotics and Automation*, San Francisco, CA.
- [15] Lewis, M. A. and Tan, K-H., 1997, "High Precision Formation Control of Mobile Robots Using Virtual Structures," *Autonomous Robots*, vol. 4, pp. 387-403.
- [16] Murray, R., Li, Z. and Sastry, S., 1993, *A Mathematical Introduction to Robotic Manipulation*, CRC Press LLC, Florida, U.S.A.
- [17] Nakamura, Y., 1991, *Advanced Robotics: Redundancy and Optimization*, Addison-Wesley Publishing Company, Inc., California, U.S.A.
- [18] Ögren, P., Egerstedt, M. and Hu, X., 2002, "A Control Lyapunov Function Approach to Multi-agent Coordination," *IEEE Transactions on Robotics and Automation*, vol. 18, no. 5, pp. 847-851.
- [19] Ögren, P., Fiorelli, E. and Leonard, N. E., 2002, "Formations with a Mission: Stable Coordination of Vehicle Group Maneuvers," *Proceedings of 15th International Symposium on Mathematical Theory of Networks and Systems*, Notre Dame, IN.
- [20] Olfati-Saber, R. and Murray, R., 2002, "Graph Rigidity and Distributed Formation Stabilization of Multi-Vehicle Systems," in *Proceedings of the 41st Conference on Decision and Control*, Las Vegas, NV.
- [21] Olfati-Saber, R. and Murray, R. M., 2003, "Flocking with Obstacle Avoidance: Cooperation with Limited Communication in Mobile Networks," in *Proceedings of 42nd IEEE Conference on Decision and Control*, Maui, Hawaii.
- [22] Ostrovskaya, S., 2001, *Dynamics of Quasiholonomic and Nonholonomic Reconfigurable Rolling Robots*, Ph.D thesis, McGill University, Montreal.
- [23] Park, F.C. and Kim, J.W., 1996, "Kinematic Manipulability of Closed Chains", *Recent Advances in Robot Kinematics*, J. Lenarcic and V. Parenti-Castelli, eds., Kluwer Academic Pub., pp. 99-108.
- [24] Park, F. and Kim, J., 1998, "Manipulability and Singularity Analysis of Multiple Robot Systems: A Geometric Approach," *Proceedings of the 1998 IEEE International Conference on Robotics and Automation*, vol.2, pp. 1032 -1037, Leuven, Belgium.
- [25] Parker, L. E., 1998, "Alliance: An Architecture for Fault Tolerant Multirobot Cooperation," *IEEE Transactions on Robotics and Automation*, vol. 14, no. 2, pp. 220-40.

- [26] Parker, L. E., 2000, "Current State of the Art in Distributed Autonomous Mobile Robotics," in *Distributed Autonomous Robotic Systems 4*, Eds. L. E. Parker, G. Bekey, and J. Barhen, Springer-Verlag:Tokyo.
- [27] Rougeaux, S. and Zelinsky A., 2000, "A Framework for Cooperation between Autonomous Mobile Robots," *ARO Workshop 2000 on Intelligent Systems*, Canberra, Australia.
- [28] Salisbury, J. K. and Craig, J. J., 1982, "Articulated Hands: Force Control and Kinematic Issues," *The International Journal of Robotics Research*, vol. 1, no. 1, pp. 4-17.
- [29] Tsai, L., 1999, *Robot Analysis: The Mechanics of Serial and Parallel Manipulators*, John Wiley & Sons, Inc., New York, NY, U.S.A.
- [30] Wang, P. K. C., 1991, "Navigation Strategies for Multiple Autonomous Mobile Robots Moving in Formation," *Journal of Robotic Systems*, vol. 8, no. 2, pp. 177-195.
- [31] Yoshikawa, T., 1985, "Manipulability of Robotic Mechanisms," *The International Journal of Robotics Research*, vol. 4, No. 2, pp. 3-9.
- [32] Young, B., Beard, R. W., and Kelsey, J. M., 2001, "A Control Scheme for Improving Multi-vehicle Formation Maneuvers," In *Proceedings of American Control Conference*, pp. 704-709, Arlington, VA.
- [33] Zefran, M., 1996, *Continuous Methods for Motion Planning*, PhD thesis, University of Pennsylvania, Philadelphia, PA.